INDUCTIVELY COUPLED PLASMA AND ELECTRON CYCLOTRON RESONANCE PLASMA ETCHING OF InGaAlP COMPOUND SEMICONDUCTOR SYSTEM

By

JIN HONG

A DISSERTATION PRESENTED TO THE GRADUATE SCHOOL
OF THE UNIVERSITY OF FLORIDA IN PARTIAL FULFILLMENT
OF THE REQUIREMENTS FOR THE DEGREE OF
DOCTOR OF PHILOSOPHY

UNIVERSITY OF FLORIDA

1998

DEDICATED TO MY PARENTS

ACKNOWLEDGMENTS

I am giving my great thanks to my adviser, Prof. Stephen J. Pearton for his encouragement and support. My committee members C. R. Abernathy, K. S. Jones, R. K. Singh, and F. Sharifi are appreciated.

I wish to express my thanks to R. J. Shul, Lei, Pablo and Christi for their assistance at Sandia National Laboratories.

And I want to give my thanks to Dr. Y. B. Hahn for his flux modeling and good discussion.

TABLE OF CONTENTS

page

ACKNOWLEDGMENTS ... iv

LIST OF TABLES ... vii

LIST OF FIGURES ... viii

ABSTRACT ... xiii

1 INTRODUCTION ... 1

2 CAPACITIVELY COUPLED PLASMA & HIGH DENSITY PLASMA ... 6

3 ELECTRON CYCLOTRON RESONANCE AND INDUCTIVELY COUPLED PLASMA ETCHING WITH $CH_4/H_2/Ar$ CHEMISTRY ION-DRIVEN MECHANISM ... 11
3.1 Materials and Methods ... 11
3.2 Results and Discussion ... 12

4 INDUCTIVELY COUPLED PLASMA ETCHING IN Cl_2 BASED CHEMISTRIES CHEMICALLY DRIVEN MECHANISM ... 23
4.1 Materials and Methods ... 23
4.2 Results and Discussion ... 23
4.2.1 Cl_2 Chemistry ... 23
4.2.2. BCl_3 Chemistry ... 33
4.2.3. $Cl_2/BCl_3/Ar$ Chemistry ... 50

5 INDUCTIVELY COUPLED PLASMA ETCHING BASED ON NEW PLASMA CHEMISTRIES BI, AND BBr_3 ... 66
5.1 Materials and Methods ... 66
5.2 Results and Discussion ... 66

6 ELECTRON CYCLOTRON RESONANCE PLASMA ETCHING BASED ON ICl AND IBr ... 81
6.1 Results and Discussion ... 81

7 SUMMARY ... 95

LIST OF REFERENCES ... 99

BIOGRAPHICAL SKETCH 103

LIST OF TABLES

Table page

1-1 Boiling points of possible etch products (chlorides) of the InGaAlP materials system 3

7-1 Typical results for the etching of InGaAlP ternary compounds in High Density Plasma tools 96

LIST OF FIGURES

Figure page

1-1 Vapor pressure of some potential etch products based on chlorine and iodine gas chemistry as a function of temperature ... 4

2-1 Conventional RF (RIE) system ... 6

2-2 Hybrid ECR - RF system ... 8

2-3 Schematic diagram of inductive coupling ... 9

2-4 Inductively Coupled Plasma (ICP) reactor ... 10

3-1 Etch rates or sputter rates of InGaP, AlInP and AlGaP as a function of microwave source power with either $5CH_4/15H_2/10Ar$ or 40Ar discharges at the constant pressure (1.5mTorr) and dc self bias (-100V) ... 13

3-2 Etch rates and etch yields of InGaP, AlInP and AlGaP as a function of ICP source power at 4mTorr, -120V dc, $5CH_4/15H_2/10Ar$ discharges ... 14

3-3 Etch rates of InGaP, AlInP and AlGaP as a function of rf chuck power in either 2mTorr, 500W ICP, $5CH_4/15H_2/10Ar$ discharges (top) or 1.5mTorr, 800W ECR, $5CH_4/15H_2/10Ar$ discharges (bottom) ... 16

3-4 Etch rates of InGaP as a function of process pressure in either 750W ICP or 750W ECR, $5CH_4/15H_2/10Ar$ discharges at the constant dc self bias (-150V) ... 17

3-5 Figure 3-5 RMS surface roughness as a function of ICP source power in 2mTorr, -120V dc, $5CH_4/15H_2/10Ar$ discharges (top) and of dc self bias in 1.5mTorr, 800W ECR, $5CH_4/15H_2/10Ar$ discharges (bottom) ... 18

3-6 AFM scan images of InGaP in 1.5mTorr, -100V dc, $5CH_4/15H_2/10Ar$ discharges at either 800W ECR (top) or 1000W ECR (bottom) ... 20

3-7 SEM micrographs of features etched into InGaP in either 2mTorr, 350W rf, 750W ICP (top) or 1.5mTorr, 100W rf, 800W ECR (bottom) $5CH_4/15H_2/10Ar$ discharges ... 21

3-8 AES surface scan (top) and depth profile (bottom) from InGaP after etching in 1000W ICP, $5CH_4/15H_2/10Ar$ discharges at constant dc bias (-120V) and pressure (4mTorr) 22

4-1 Mass spectra in 2mTorr, -100V dc, 750W ICP Cl_2/Ar (top) or Cl_2/H_2 (bottom) discharges at the different gas compositions. 25

4-2 Etch rates of InGaP, AlInP and AlGaP (top) ar intensities of plasma species from mass spectra (center, bottom) as a function Cl_2 percentage in either Cl_2/Ar or Cl_2/H_2 discharges at fixed pressure (2mTorr), dc bias (-100V) and ICP source power (750W) 27

4-3 Etch rate of AlGaP as a function of Al composition in 2mTorr, -100V dc, 750W ICP, $5Cl_2/10Ar$ discharges 29

4-4 Etch rates (top) and etch yields (bottom) of InGaP, AlInP and AlGaP as a function of ICP source power in 2mTorr, -100V dc, $10Cl_2/5Ar$ discharges. 30

4 5 Etch rates of three ternary compound semiconductors as a function of dc self bias in 2mTorr, 750W ICP, $10Cl_2/5Ar$ discharges 32

4-6 RMS surface roughness of InGaP as a function of gas composition in either Cl_2/Ar or Cl_2/H_2 discharges at constant dc bias (-100V) and source power (750W) 34

4-7 AFM scan images of InGaP in 2mTorr, -100V dc $10Cl_2/5Ar$ discharges at either 750W ICP source power (top) or 1000W ICP source power (bottom) 35

4-8 AFM scan images of AlInP at the different rf power and source power in $10Cl_2/5Ar$ discharges 36

4-9 SEM micrographs of features etched into AlInP in 2mTorr, 1000W ICP, $10Cl_2/5Ar$ discharges (top) or 2mTorr, 750W ICP, $5Cl_2/10Ar$ discharges (bottom) at constant dc bias (100V) 37

4 10 AES surface scan (top) and depth profile (bottom) from InGaP after etching in 2mTorr, -100V dc, 750W source power, $10Cl_2/5Ar$ discharges 38

4-11 AES surface scan (top) and depth profile (bottom) from InGaP after etching in 2mTorr, -100V dc, 750W source power, $5Cl_2/10H_2$ discharges. 39

4 12 Etch rates of InGaP, AlInP and AlGaP as a function of gas composition in either BCl_3/Ar (top) or BCl_3/H_2 (bottom) at the fixed source power (750W) and pressure (2mTorr) with two different dc biases (-100V, -200V) 41

4 13 Mass spectra of plasma species from both $5BCl_3/10Ar$ and $5BCl_3/10H_2$ discharges at fixed source power (750W), dc bias (-100V) and pressure (2mTorr) 43

4-14 Optical emission spectra in either $5BCl_3/10Ar$ or $5BCl_3/10H_2$ discharges at fixed source power (750W), dc bias (-200V) and pressure (2mTorr) 44

4-15 Optical emission spectra in 2mTorr, 1000W ICP, $5BCl_3/10Ar$ discharges at -200V dc (top) and normalized intensity as a function of source power (bottom) 45

4-16 Etch rates (top) and etch yields of InGaP, AlInP and AlGaP as a function of ICP source power in 2mTorr, $5BCl_3/10Ar$ discharges at two different ion energies. 47

4-17 Etch rates of InGaP, AlInP and AlGaP as a function of dc self bias in 2mTorr, 750W ICP, $5BCl_3/10Ar$ discharges. 48

4-18 AFM surface scan images of InGaP in 2mTorr, 750W ICP, -100V dc, BCl_3/Ar or BCl_3/H_2 discharges at the different gas compositions. 49

4-19 SEM micrographs of features etched into InGaP in different ion energies and gas compositions 51

4-20 SEM micrographs for AlInP etched in either -100V dc, $5BCl_3/10Ar$ discharges (top) or -200V dc, $10BCl_3/5Ar$ discharges (bottom) at fixed source power (750W) and process pressure (2mTorr) 52

4-21 AES surface scans from AlInP before and after etching in 2mTorr, $5BCl_3/10Ar$ discharges at the different source powers and ion energies 53

4-22 Optical emission spectra from 2mTorr, $Cl_2/BCl_3/5Ar$ discharges as a function of Cl_2/BCl_3 composition at fixed source power (500W) and dc bias (-150V) 55

4-23 Mass spectra from 2mTorr, $Cl_2/BCl_3/5Ar$ discharges as a function of Cl_2/BCl_3 composition at fixed source power (750W) and dc bias (-150V) 56

4-24 Etch rates of InGaP and AlInP (top) and normalized intensity of optical emission spectra as a function of gas composition in 2mTorr, -150V dc, 500W ICP, $Cl_2/BCl_3/5Ar$ discharges 57

4-25 Etch rates of InGaP and AlInP as a function of source power in 2mTorr, $32Cl_2/8BCl_3/5Ar$ discharges at -150V dc bias 59

4-26 Etch rates of InGaP and AlInP (top), and normalized intensities from optical emission spectra (bottom) as a function of dc self bias in 2mTorr, 500W ICP, $32Cl_2/8BCl_3/5Ar$ discharges 60

4-27 Etch rate of InGaP and AlInP (top), and Normalized intensities from mass spectra (bottom) as a function of process pressure in $32Cl_2/8BCl_3/5Ar$ discharges at fixed source power (750W) and dc self bias (-150V) 61

4-28 RMS roughness of InGaP after etching in 2mTorr, -150V dc, $32Cl_2/8BCl_3/5Ar$ discharges as a function of ICP source power 63

4-29 AFM surface scan images of AlInP etched in 2mTorr, $32Cl_2/8BCl_3/5Ar$ discharges at the different source power and ion energy 64

4-30 SEM micrographs of features etched into InGaP (top, left or bottom, left and right) and AlInP (top, right) with 750W (top) or 500W (bottom) ICP and -150V dc (top), 300V dc (bottom, left) or -400V dc (bottom, right) in $32Cl_2/8BCl_3/5Ar$ discharges The photoresist mask (bottom, left) has been removed and SiN_x masks are still in phase (top, left and right, and bottom, right) 65

5-1 Optical emission spectrum from Bl_3 discharge. 68

5-2 Etch rates (top) and etch yields (bottom) for InGaP, AlInP and AlGaP in 750W source power, 5mTorr discharges of $4Bl_3/6Ar$ or $4BBr_3/6Ar$ discharges as a function of chuck dc bias. 69

5-3 Etch rates of InGaP, AlInP and AlGaP in (top) Bl_3/Ar discharges (750W source power, 150W rf chuck power) as a function of plasma composition, (center) BBr_3/Ar discharges (750W source power, 350W rf chuck power) as a function of plasma composition, or (bottom) etch selectivity of InGaP over AlInP under these conditions 70

5-4 Etch rates (top) and etch yields (bottom) for InGaP, AlInP and AlGaP in $4Bl_3/6Ar$, 150W rf power, 5mTorr discharges as a function of ICP source power 72

5-5 Etch rates (top) and etch yields (bottom) for InGaP, AlInP and AlGaP in $4BBr_3/6Ar$, 350W rf power, 5mTorr discharges as a function of ICP source power 73

5-6 AFM scans from InGaP etched in 750W source power, Bl_3/Ar discharges with different compositions and rf powers. 75

5-7 AFM scans from InGaP etched in 750W source power, 350W rf power BBr_3/Ar discharges with different compositions 76

5-8 SEM micrographs of features etched into InGaP using 750W source power discharges of (top left) $2Bl_3/8Ar$, 250W rf power, (top right) $4Bl_3/6Ar$, 150W rf power, (bottom left) $8BBr_3/2Ar$, 350W rf power and (bottom right) $10BBr_3$, 350W rf power The SiN_x masks are still in place in all cases. 77

5-9 AES surface scan (top) and depth profile (bottom) from AlInP after etching in 5mTorr, $8BBr_3/2Ar$ discharges at fixed source power (750W) and rf chuck power (350W) 78

5-10 Etch selectivities of InGaP over SiO_2 and SiN_x in (top) $4BBr_3/6Ar$ discharges, 350W rf power, 5mTorr, as a function of ICP source power, and (bottom) in $4BI_3/6Ar$ or $4BBr_3/6Ar$, 750W source power, 5mTorr discharges, as a function of rf power ... 79

6-1 Etch rates of ternary alloys as a function of plasma composition in ICl/Ar or IBr/Ar discharges (1000W microwave power, 150W rf power, 1 5mTorr) ... 82

6-2 Etch rates of ternary alloys as a function of microwave power in 4ICl/4Ar or 4IBr/4Ar discharges (150W rf power, 1 5mTorr) ... 84

6-3 Etch rates of ternary alloys as a function of rf power in 4ICl/4Ar or 4IBr/4Ar discharges (1000W microwave power, 1.5mTorr) ... 86

6-4 AFM scans of InGaP (top) or AlInP (bottom) after etching in 4ICl/4Ar, 1 5mTorr discharges at 1000W microwave power, 150W rf (top, left), 600W microwave, 150W rf (top, right), 800W microwave, 150W rf (bottom, left), or 1000W microwave, 250W rf (bottom, right) ... 87

6-5 AFM scans of AlInP after etching in 1000W microwave, 150W rf, 1 5mTorr discharges of 2IBr/6Ar (top), 4IBr/4Ar (center), or 8IBr (bottom) ... 88

6-6 RMS surface roughness of InGaP and AlInP samples after etching in 1000W microwave, 150W rf, 1 5mTorr IBr/Ar discharges as a function of plasma composition ... 89

6-7 AES surface scan of AlInP after etching in a 1000W microwave, 150W rf, 1.5mTorr discharges of 8IBr ... 90

6-8 SEM micrographs of features etched into InGaP (top) or AlInP (bottom) with a 750W microwave, 150W rf, 1 5mTorr discharges of 4IBr/4Ar The photoresist mask has been removed. ... 92

6-9 SEM micrographs of features etched into InGaP (top) or AlInP (bottom) with 1000W microwave, 250W rf, 1 5mTorr discharges of 4ICl/4Ar The photoresist masks have been removed ... 93

6-10 Etch rates of $Al_xGa_{1-x}P$ alloys as a function of Al compositions in 1000W microwave, 150W rf, 1 5mTorr discharges of 4IBr/4Ar ... 94

Abstract of Dissertation Presented to the Graduate School
of the University of Florida in Partial Fulfillment of the
Requirements for the Degree of Doctor of Philosophy

INDUCTIVELY COUPLED PLASMA AND ELECTRON CYCLOTRON RESONANCE PLASMA ETCHING OF InGaAlP COMPOUND SEMICONDUCTOR SYSTEM

By

Jin Hong

December 1998

Chairman: Stephen J. Pearton
Major Department: Materials Science and Engineering

Current and future generations of sophisticated compound semiconductor devices require the ability for submicron scale patterning. The situation is being complicated since some of the new devices are based on a wider diversity of materials to be etched. Conventional RIE (Reactive Ion Etching) has been prevalent across the industry so far, but has limitations for materials with high bond strengths or multiple elements. In this dissertation, we suggest high density plasmas such as ECR (Electron Cyclotron Resonance) and ICP (Inductively Coupled Plasma), for the etching of ternary compound semiconductors (InGaP, AlInP, AlGaP) which are employed for electronic devices like heterojunction bipolar transistors (HBTs) or high electron mobility transistors (HEMTs), and photonic devices such as light emitting diodes (LEDs) and lasers. High density plasma sources, operating at lower pressure, are expected to meet target goals determined in terms of etch rate, surface morphology, surface stoichiometry, selectivity, etc. The

etching mechanisms, which are described in this dissertation, can also be applied to other III-V (GaAs based, InP-based) as well as III-Nitride since the InGaAlP system shares many of the same properties

CHAPTER 1
INTRODUCTION

The InGaAlP semiconductor system, which consists of InGaP, AlInP and AlGaP, is used in a number of applications due to its interesting properties. The first motivation of investigating these materials is that $In_xGa_{1-x}P$ and $Al_xIn_{1-x}P$ ($x \sim 0.5$) are lattice matched to GaAs (lattice constant is 0.6532Å), which results in the achievement of heteroepitaxy.[1] In addition, InGaP has many attractive properties compared with AlGaAs, which is now being used in HBT devices. InGaP has a larger valence band discontinuity ($\Delta E_v = 0.3eV$) leading to improved γ (carrier injection efficiency) in HBTs (Heterojunction Bipolar Transistors), lower densities of DX centers, lower surface recombination velocity and, finally, it is not prone to oxidation due to its Al-free composition. All these properties make InGaP a potential substitute for AlGaAs in HBTs or HEMTs (High Electron Mobility Transistor). Beyond that, the InGaAlP system displays a wide range of bandgaps from $In_{0.49}Ga_{0.51}P$ (1.9eV) to $(Al_xGa_{1-x})_{0.51}In_{0.49}P$ ($x \sim 0.66$, 2.3eV), which are suitable for visible range LEDs and lasers.[2-20]

For the pattern transfer of these materials, some challenges must be solved. Issues for the etching of this system can be divided into two parts. The first part lies in the intrinsic properties of materials themselves. For InGaP and AlInP, the group V element (P^2) is lighter than the group III elements (In, Ga). Thus, phosphorous is sensitive to preferential sputtering during the etching process, giving rise to nonstoichiometric surfaces. In addition, AlGaP has a higher melting point (2282K) than either InGaP

(1538K) or AlInP (2079K), which is a good indication of their average bond strengths [23] This high bond strength usually leads to very slow etch rates. The universal etchant for the etching of In-containing semiconductors has been the methane-hydrogen-based chemistry because of its ability to produce volatile etch products However, the etch rates with this chemistry are too low to maintain good throughput. Secondly, the presence of methane produces polymer deposition on the mask and within the chamber [24,25] In addition, the presence of hydrogen in the plasma results in electrical passivation of near-surface dopants [26-28] While these problems can be avoided using chlorine-based chemistries, which is generally used for Ga-based semiconductors, it is generally believed that an involatile etch product of indium ($InCl_3$: b.p. 600°C) rapidly forms a thick reaction layer on the surface with the result of low etch rate and rough surface. Table 1-1 shows boiling points of possible etch products (chlorides) for the InGaAlP materials system. It turns out that there is a big difference in boiling points between group III (Indium) and group V etch products. This different volatility of group III (Indium) and group V makes etching of In-containing materials difficult in terms of obtaining high etch rate and smooth or stoichiometric surfaces. The only way to solve this in conventional RIE (Reactive Ion Etching) is to heat the sample while etching. This approach is not desirable because the elevated temperature precludes use of photoresist as the mask and presents reproducing problems. The other approach we took is use of high density plasmas. It is expected that the high ion density available in the plasma can sputter away involatile etch products efficiently with the achievement of high etch rate and smooth surface morphology [29-33]

In addition, we examined new gas chemistries based on iodine and bromine under high density plasma conditions. It has long been recognized that I_2-based gas mixtures might be advantageous for dry etching In-containing compound semiconductors because of higher volatility of InI_x species relative to $InCl_3$, as will be described below. Evaporation rate can be expressed as

$$v_e=\alpha[M_A/2\pi RT]^{1/2}P_A \quad (1\text{-}1)$$

$$P_A \text{ (vapor pressure)}=C_A e^{-\Delta H/RT} \quad (1\text{-}2)$$

$$\text{And so, } v_e=\alpha C_A[M_A/2\pi RT]^{1/2} e^{-\Delta H/RT} \quad (1\text{-}3)$$

Table 1-1 Boiling points of possible etch products (chlorides) of the InGaAlP materials system

Species	Boiling points (°C)
$GaCl_3$	201
$InCl_3$	600
$AlCl_3$	183
PCl_3	76

Figure 1-1 shows vapor pressure[23] of some potential etch products as a function of temperature. As indicated in equation (1-2), the slope of this plot is enthalpy of vaporization, which is equivalent to activation energy for desorption (E_d). As expected, $InCl_3$ has much higher value of E_d (37.8kcal/mole) than $GaCl_3$, leading to the lower evaporation rate of $InCl_3$, while etch product (InI_x) based upon iodine provided lower energy barrier (20.2kcal/mole) for the desorption enhancing its evaporation. Pure I_2 is a

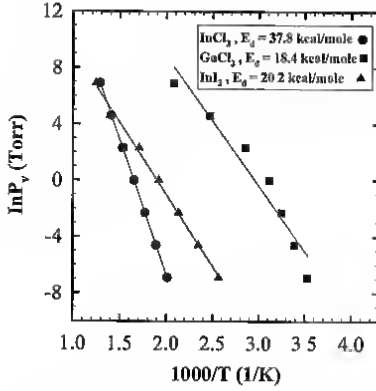

Figure 1-1. Vapor pressure of some potential etch products based on chlorine and iodine gas chemistry as a function of temperature.

solid requiring heating to produce a practical flow rate for etch processes (m.p. 113.5°C). Alternatives such as HI, CH_3I, C_2H_5I and C_3H_7I have all been investigated previously. All of these have drawbacks-HI has a shelf-life of about 6 months before decomposing to H_2 and I_2, while the methyl-, ethyl- and propyl- iodide are unsuitable for high density plasma sources because of excessive polymerization.[26] Bromine-based plasma chemistries have also not received sufficient attention. HBr has been shown to selectively etch InGaAs

over InAlAs [35,36] Pure Br_2 is extremely corrosive in the presence of even minute quantities of water vapor in gas lines, mass flow controllers or pumping systems It is therefore of interest to investigate an alternative source of I_2 and Br_2 for etching of InGaAlP in this thesis, a comparison of high density plasmas such as ECR (Electron Cyclotron Resonance) and ICP (Inductively Coupled Plasma) based on several gas chemistries (CH_4/H_2, Cl_2, BCl_3, ICl, BI_3, IBr, BBr_3) will be described for the etching of InGaAlP semiconductor system.

CHAPTER 2
CAPACITIVELY COUPLED PLASMA & HIGH DENSITY PLASMA

Figure 2-1 shows a conventional RIE system. Radiofrequency power is deposited into the thin sheath region by capacitive coupling. The electrons, which are subject to rf power applied to the electrode, will be accelerated at the sheath regions changing direction upward and downward. The collisions that electrons undergo with gas molecules contribute to sustaining the plasma. The motion range of electrons is large compared to that of ions due to their smaller mass. Electrons may be lost to the electrode, which will take on a negative DC bias because of the charge transferred from the electrons. This self bias may lead to damage to the sample by subsequent ion bombardment, giving rise to electrical or optical degradation.

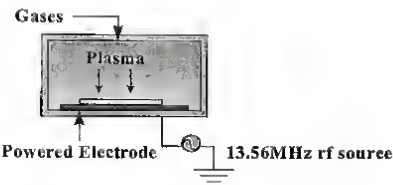

Figure 2-1. Conventional RF (RIE) system

In addition, ion flux is coupled with ion energy Thus, high ion flux can be achieved only at the expense of surface degradation due to the high ion energy

On the other hand, the mechanism behind achieving a high density plasma is electron confinement. As described in Figure 2-2, Electron Cyclotron Resonance (ECR) takes advantage of an external magnetic field and a resonance effect to confine electrons The frequency of orbital motion of electrons, confined under the action of an external magnetic field (875 Gauss) is equivalent to the drive frequency of 2 45 GHz leading to the occurrence of resonance, called electron cyclotron resonance, if this frequency of power is applied to the plasma. Subjected to this condition, electrons will be accelerated extending their mean free path more and more before getting lost to the electrode. The power is coupled into the electrons efficiently through the dielectric window Now that ion density is decoupled with ion energy due to the trapped electrons, ECR can provide high ion density ($10^{11} \sim 10^{13}$ cm^{-3}) compared with RIE ($\sim 10^{9}$ cm^{-3}) without inducing high damage to the sample. Moreover ion energy can be controlled separately by applied chuck bias Furthermore, ECR discharges are capable of low pressure operation due to its efficient dissociation of gases to form the discharge

Another high density plasma, Inductively Coupled Plasma (ICP), has become popular in semiconductor processing. As shown in Figure 2-4, the configuration is simple compared to ECR reactor RF current circulating around the chamber in opposite directions causes an alternating magnetic field in the upward and downward directions. ($I_{RF} \rightarrow B_{RF}$) It is this change in rate of magnetic field that induces a RF electric filed ($dB_{RF}/dT \rightarrow E_{RF}$) (See Figure 2-3) This RF field (E_{RF}) will accelerate the electrons into the circular path, confining them in a circular motion The power transfer through the

dielectric window by inductive coupling is efficient, leading to high ion density The plasma, first formed in the shape of a ring following the path of electrons, will diffuse to

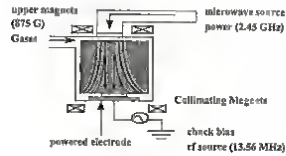

Figure 2-2 Hybrid ECR - RF system

the center of the chamber and then downward toward the sample As long as the capacitively coupled component is absent, or at least small, the electrons trapped themselves in a circular path, will have only a small chance to be lost to the chuck resulting in low DC self bias Ion energy, separate from the ion flux, can be controlled by applying another rf source at the chuck Unlike ECR, ICP does not use resonance or microwave power source Hence, it can provide advantages over ECR such as easier turning and low price Also, it is believed to be easy to scale-up for large wafer processing.

High density plasmas such as ECR and ICP achieve decoupling of ion energy and ion density by electron confinement Then, what kind of advantages can high density plasmas produce for etch processing? First, higher dissociation of gases to ignite plasma,

due to the longer mean free path or mean lifetime of electrons, which are trapped inside the plasma, can provide high ion density and large concentrations of atomic radicals. This will lead to high etch rate. Secondly, fewer electrons are lost to the wall or electrode compared to RIE, and thus less ion damage is induced. The last advantage is low pressure operation. This makes it possible to get anisotropic etching and will be major factor as the feature size etched becomes smaller.

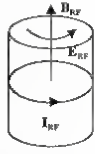

Figure 2-3 Schematic diagram of inductive coupling

In this dissertation we describe use of ICP and ECR reactor and different plasma chemistries, for the etching of the InGaAlP system. The predominant etch mechanism, i.e. physical, chemical or ion-enhanced, has been determined in each case by measurement of etch yield.

The etching was characterized by a variety of methods, which include stylus profilometry for etch rates, Auger Electron Spectroscopy (AES) for near-surface stoichiometry, and Scanning Electron Microscopy (SEM) and Atomic Force Microscopy

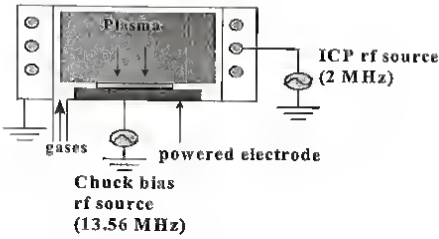

Figure 2-4 Inductively Coupled Plasma (ICP) reactor

(AFM) for surface morphology The active species in the plasma were measured by Optical Emission Spectroscopy (OES) and mass spectrometry

The yields were based on a model developed by Y. B. Hahn. The model provides ion flux and ion velocity (Bohm velocity) at the sheath edge, leading to the calculation of etch yield. Etch yield describes the atoms removed by an ion during the etch process and can be a good indicator in understanding the etch mechanism

CHAPTER 3
ELECTRON CYCLOTRON RESONANCE AND INDUCTIVELY COUPLED PLASMA ETCHING WITH $CH_4/H_2/Ar$ CHEMISTRY ION DRIVEN MECHANISM

3.1 Materials and Methods

The $In_{0.5}Ga_{0.5}P$ and $Al_{0.5}In_{0.5}P$ were grown lattice-matched to GaAs substrates by either metal organic molecular beam epitaxy (MOMBE)[37] or metal organic chemical vapor deposition (MOCVD)[38] using trimethylindium, trimethylamine alane, triethylgallium and phosphine Layers were nominally undoped ($p \leq 2\times10^{15}$ cm^{-3}) and were typically 1-2 μm thick. The compositions were confirmed by double crystal X-ray diffraction and photoluminescence [12,13] The $Al_{0.5}Ga_{0.5}P$ was grown on Si by MOMBE and was carbon doped ($p \sim 10^{18}$ cm^{-3})

The samples were patterned with AZ5209E photoresist in a resolution test pattern with lines and spaces of 1-100μm All the etching was performed in both Plasma Therm 790 ICP system and Plasma Therm SLR 770 system For 790 system, the plasma is generated in a 3 turn planar ICP source (0 1500W) operating at 2MHz The electrode was biased through application of rf (13 56 MHz) power (0-450W) For 770 system, a low profile ECR source (Astex 4400) operating at 2 45GHz was powered between 400 100W, with an upper magnet of 170A and a lower collimating magnet current of 40A The samples were thermally bonded to a mechanically clamped Si carrier wafer The process pressure was varied from 2-15mTorr at a total gas flow rate of 15 standard cubic

centimeter per minute (sccm). Etch rates were obtained from stylus profilometry after removal of the resist in acetone. Surface roughness was examined by atomic force microscopy (AFM). The near-surface chemistry was investigated by Auger Electron Spectroscopy (AES) in a Perkin Elmer system using a 0.5keV probe beam. Depth profiling was performed in these experiments with a 2keV Ar^+ ion beam, producing a sputter rate of ~70Å·min^{-1}.

3.2. Results and Discussion

Figure 3-1 shows etch rates or sputter rates of InGaP, AlInP and AlGaP as a function of microwave source power in either $5CH_4/15H_2/10Ar$ or 30Ar discharges at constant pressure and dc self bias. Microwave source power controls ion flux and atomic neutral density by creating more efficient dissociation of the plasma. The general trend in etch rates in both discharges is higher etch rates for all three semiconductors at the higher microwave power due to the higher abundance of dissociated neutrals and ions in the plasma. The first thing we note here is that the etch rates for all materials, achieved in $CH_4/H_2/Ar$ discharges, are lower at the whole range of microwave source power investigated than the sputter rate. Secondly, Al containing materials (AlInP, AlGaP) showed slow etching compared to InGaP. The lack of chemical enhancement with $5CH_4/15H_2/10Ar$ chemistry may be related with the fact that the generation of methyl radicals in the plasma is not efficient enough for the etching, or competition between polymer deposition and etching limits etch process.[11,38,40] We tend to eliminate the latter since polymer residues were not detected on the surface. Inductively Coupled Plasma (ICP) shows a similar trend to Electron Cyclotron Resonance (ECR). Figure 3-2 shows etch rates and etch yield as a function of ICP source power with the same gas chemistry

($CH_4/H_2/Ar$) at constant dc self bias and pressure. Etch rates, obtained under ICP, are comparable to the case of ECR. Etch yield calculated remained low values constantly irrespective of source power. The increase in etch rates with $CH_4/H_2/Ar$ chemistry, therefore, is likely to result from the increase of the ion flux at higher source power, which implies an ion-assisted mechanism.

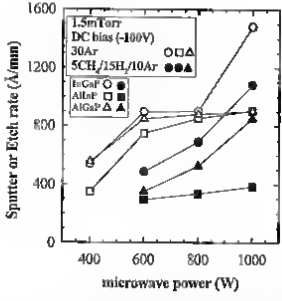

Figure 3-1. Etch rates or sputter rates of InGaP, AlInP and AlGaP as a function of microwave source power with either $5CH_4/15H_2/10Ar$ or 40Ar discharges at the constant pressure (1.5mTorr) and dc self bias (-100V).

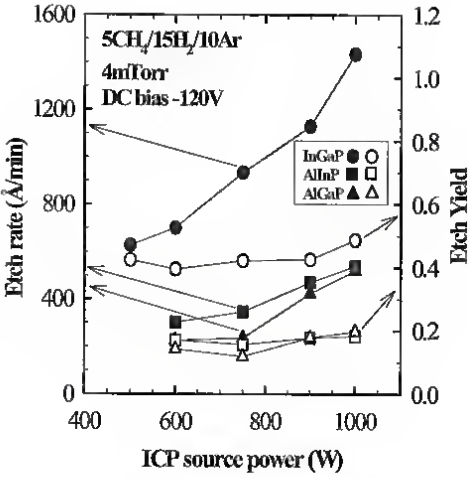

Figure 3-2 Etch rates and etch yields of InGaP, AlInP and AlGaP as a function of ICP source power at 4mTorr, -120V dc, $5CH_4/15H_2/10Ar$ discharges

In addition to the ion flux, the ion energy, controlled by rf chuck bias, has a significant impact on the etch rates As shown in Figure 3-3, etch rates of all ternary compounds increase as the rf chuck bias is increased under both ICP (top) and ECR (bottom) conditions The increase in rf chuck bias controls the potential between chuck and plasma resulting in higher ion energy. High ion energy along with high ion flux can provide a good condition for the desorption of etch products as well as the bond breaking of the target materials

Pressure controls the relative contributions of the physical and chemical components of the etching As pressure is increased, chemical component outweighs physical component due to the low electron energy and ionization efficiency. Figure 3-4 shows etch rate dependence on the pressure for InGaP under both ICP and ECR at constant dc self bias and source power The etch rates dropped above 2mTorr and kept constant values thereafter in both cases This result confirms once again the ion-driven mechanism of the $CH_4/H_2/Ar$ chemistry for the etching of InGaP The dominance of chemical component at high pressure led to the suppression of etching above 2mTorr

Surface roughness depends upon both ICP source power and ion energy In conventional RIE etching, the surface roughens with an increase in etch rate[139] However, Inductively Coupled Plasma (ICP) etching produces smooth surface even at high etch rates As shown in Figure 3-5 (top), root-mean-square (RMS) roughness obtained from AFM for InGaP decreases at higher ICP source power in $5CH_4/15H_2/10Ar$ discharges at constant pressure (2mTorr) and dc self bias (-120V). We believe this results from the higher ion flux available Figure 3 5 (bottom) shows RMS roughness of InGaP as a function of dc self bias under both ICP (500W) and ECR (800W) conditions Surface

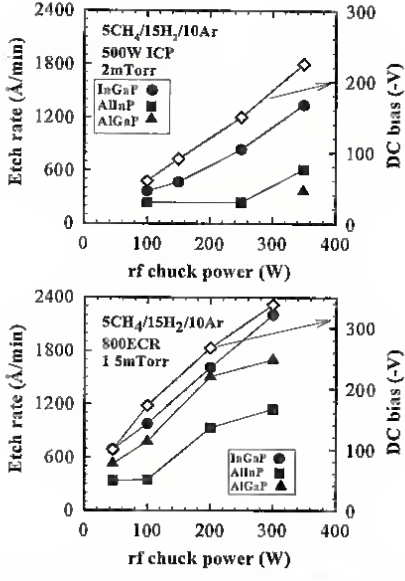

Figure 3-3 Etch rates of InGaP, AlInP and AlGaP as a function of rf chuck power in either 2mTorr, 500W ICP, $5CH_4/15H_2/10Ar$ discharges (top) or 1.5mTorr, 800W ECR, $5CH_4/15H_2/10Ar$ discharges (bottom)

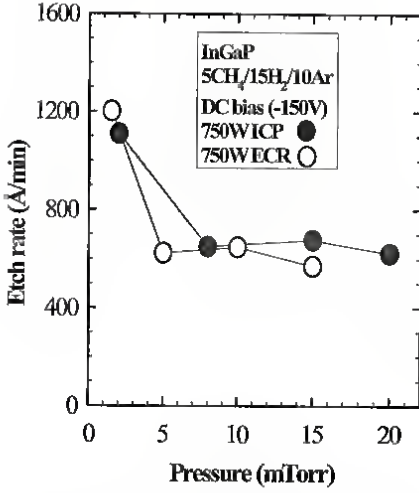

Figure 3 4 Etch rates of InGaP as a function of process pressure in either 750W ICP or 750W ECR, $5CH_4/15H_2/10Ar$ discharges at the constant dc self bias (-150V)

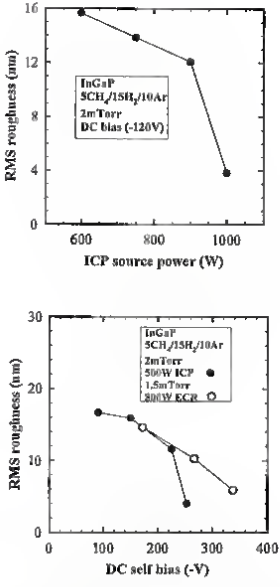

Figure 3-5 RMS surface roughness as a function of ICP source power in 2mTorr, -120V dc, $5CH_4/15H_2/10Ar$ discharges (top) and of dc self bias in 1.5mTorr, 800W ECR, $5CH_4/15H_2/10Ar$ discharges (bottom)

morphology of InGaP improved with higher ion energy in both ICP and ECR cases, probably due to the enhanced ion sputtering of etch products. AFM scans images of InGaP with −100V dc, $5CH_4/15H_2/10Ar$ discharges at the different microwave source powers are shown in Figure 3-6. A Smoother surface was obtained with higher ion flux from RMS value of 22.4nm at 800W ECR to 5.4nm at 1000W ECR. SEM pictures of InGaP with $CH_4/H_2/Ar$ chemistry are shown in Figure 3-7 at 2mTorr, 350W rf, 750W ICP (top) or 1.5mTorr, 100W rf, 800W ECR (bottom) discharges. The etched surface was rough with tilted sidewalls (top) and In droplets on the surface were observed. Reduced rf power led to more sloped sidewalls due to the suppressed ionic component (bottom).

Turning to the near-surface chemistry, Figure 3-8 shows AES surface scan (top) and depth profile (bottom) from InGaP after etching in $5CH_4/15H_2/10Ar$ discharges at the ICP source power (1000W) that maximizes etch rate (1435Å/min). There is oxygen present from the native oxide that grows on the sample during the transfer from the etch reactor to the AES chamber, and also carbon from the same exposure to ambient air. There is indium enrichment (In droplet formation) apparent in the near surface region, and this may confirm the claim regarding inefficient generation of reactive radicals in the plasma with this chemistry. The depletion of phosphorous from the surface extended into the sample around 100Å, probably due to the high volatility of the P etch product, phosphine (PH_3).

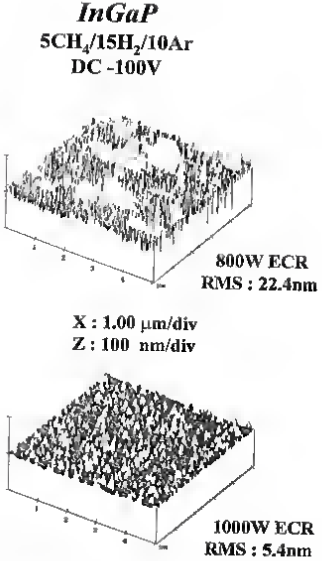

Figure 3-6 AFM scan images of InGaP in 1.5mTorr, –100V dc, $5CH_4/15H_2/10Ar$ discharges at either 800W ECR (top) or 1000W ECR (bottom)

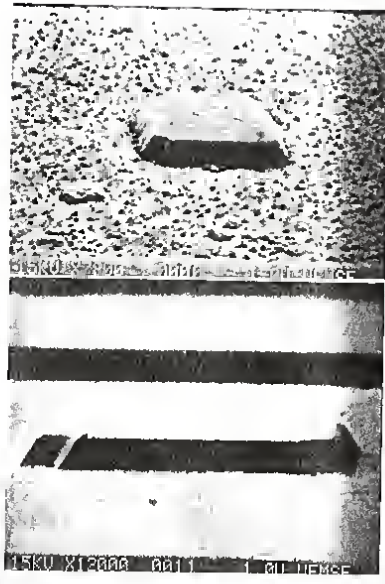

Figure 3-7 SEM micrographs of features etched into InGaP in either 2mTorr, 350W rf, 750W ICP (top) or 1.5mTorr, 100W rf, 800W ECR (bottom) $5CH_4/15H_2/10Ar$ discharges

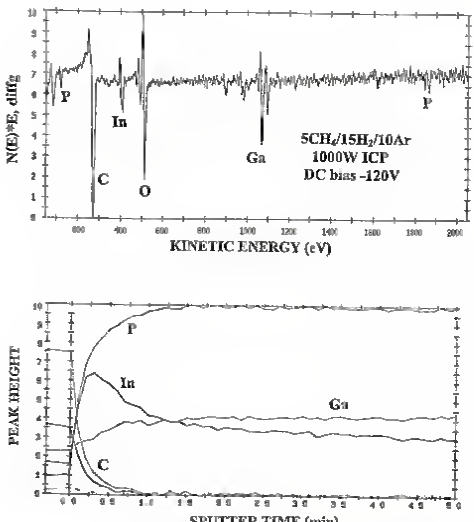

Figure 3-8 AES surface scan (top) and depth profile (bottom) from InGaP after etching in 1000W ICP, $5CH_4/15H_2/10Ar$ discharges at constant dc bias (-120V) and pressure (4mTorr)

CHAPTER 4
INDUCTIVELY COUPLED PLASMA ETCHING IN Cl_2-BASED CHEMISTRIES : CHEMICALLY DRIVEN MECHANISM

4.1. Materials and Methods

The samples were patterned with AZ4330 photoresist. Etch selectivities to resist were typically 3-6 for all of our conditions. All the etching was performed in a Plasma Therm 790 ICP system. The plasma is generated in a 3-turn planar ICP source (0-1500W) operating at 2MHz. The electrode was biased through application of rf (13.56 MHz) power (0-400W). The process pressure was varied from 2-15mTorr for a total gas flow rate of 15 standard cubic centimeter per minute (sccm). Etch rates were obtained from stylus profilometry of the craters after removal of the resist in acetone. Surface morphologies were examined by both Scanning Electron Microscopy (SEM) and Atomic Force Microscopy (AFM). The near surface atomic composition was measured by Auger Electron Spectroscopy (AES). Plasma species were detected by Optical Emission Spectroscopy (OES) and Quadruple Mass Spectroscopy (QMS).

4.2. Results and Discussion

4.2.1. Cl_2 Chemistry

Figure 4-1 shows the comparison of plasma species obtained from mass spectroscopy measurements in either Cl_2/Ar (bottom) or Cl_2/H_2 (top) discharges at fixed source power (750W), dc bias (-100V) and pressure (2mTorr). Dominant species in

Cl_2/Ar mixture were atomic chlorine (35~37AMU) and molecular chlorine in the range from 70 to 74AMU. Most chlorine species increased in intensity with Cl_2 concentration, while chlorine ion $37Cl^{2+}$, detected at 18.5AMU, did not show any variation in intensity regardless of gas composition change. On the contrary, adding hydrogen created new species (HCl) with suppression of chlorine molecules. HCl, with its components in 35~38AMU, has high thermodynamic stability relative to Cl and Cl_2.[42] Two possible gas phase reaction mechanisms to produce HCl are as follows

$$Cl+H_2 \rightarrow H+HCl,\ \Delta H°_{298}=-4.2kJ/mole,\ E_a=21.3kJ/mole \quad (4\text{-}1)^{[42]}$$

$$Cl_2+H \rightarrow Cl+HCl,\ \Delta H°_{298}=-189.1kJ/mole,\ E_a=5.0kJ/mole \quad (4\text{-}2)^{[42]}$$

These reactions can proceed easily in the plasma to produce HCl, due to the low activation energy barriers for both reactions. Maximum intensities for HCl (35~38AMU) occurred at 33.3% Cl_2 concentration. Above that composition, intensities of HCl decreased with chlorine molecule appearance.

Figure 4-2 shows the etch rate dependence of $In_{0.5}Ga_{0.5}P$, $Al_{0.1}In_{0.9}P$ and $Al_{0.5}Ga_{0.5}P$ (top), and change of intensities for plasma species (center, bottom) on discharge composition for either Cl_2/Ar or Cl_2/H_2 at fixed pressure (2mTorr), ICP source power (750W) and dc self-bias (-100V). The rf power was varied between 150-175W to hold dc bias constant. The general trend in both discharges is for the etch rates to go through a maximum with percentage Cl_2 in the discharge. The pure Ar sputter rates are low for all these materials, and as Cl_2 is added, the etch rates rise rapidly, indicating a strong chemical enhancement. However, beyond particular plasma compositions, the etch rates fall and are low again for pure Cl_2 discharges.

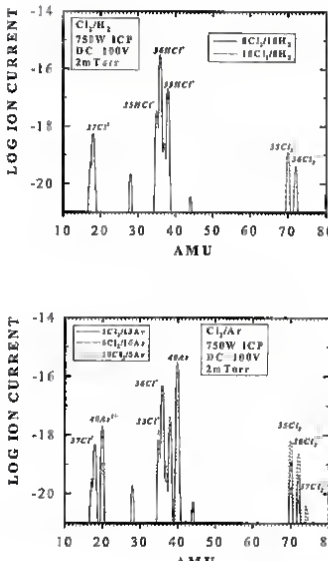

Figure 4-1 Mass spectra in 2mTorr, -100V dc, 750W ICP Cl_2/Ar (top) or Cl_2/H_2 (bottom) discharges at the different gas compositions

We interpret this behavior in terms of a competition between formation of chlorinated etch products and their removal by ion-assisted desorption. As indicated in Figure 4-2 (center), atomic chlorines and molecular chlorines increase at the expense of Ar with Cl_2 concentration. At optimized ion-to neutral ratios of these etch products there will be a balance between the formation and removal rates of these etch products [10,1,44-46] At high atomic chlorine conditions, there will be a build-up of a thick selvedge or reaction layer which is not efficiently removed by ion sputtering. This is the typical situation in Cl_2-based reactive ion etching of In-containing III-V semiconductors,[1,47-50] or of strongly bonded materials like AlGaP. For Cl_2/H_2, the etch rate maximum occur at relatively low Cl_2 compositions, and the maximum rate obtained for InGaP in Cl_2/H_2 is significantly faster than with Ar addition. We believe this is due to the creation of new species (HCl) in the plasma since the etch rate of InGaP is consistent with HCl intensity change, as represented in Figure 4-2 (bottom)

The etch rate of AlGaP was found to be a strong function of AlP mole fraction, and this is useful when considering structures in which an etch stop layer is required. For the x=0.5 alloys, AlGaP has a higher melting point (2282K) than either InGaP (1536K) or AlInP (2079K) which is a good indication of higher bond strength for AlGaP, and this difference in bond strength increases as the AlP mole fraction in AlGaP is increased. The standard enthalpy of formation for AlP (-39.6kcal/mole) is higher than that for GaP (-30kcal/mole) [51] We observed reduced etch rate of $Al_xGa_{1-x}P$ as the Al composition was increased, from ~1100 Å min^{-1} for $Al_{0.06}Ga_{0.94}P$ to ~160 Å min^{-1} for $Al_{0.9}Ga_{0.1}P$ in $5Cl_2/10Ar$, 750W source power, −100V dc bias discharges, as shown in Figure 4-3

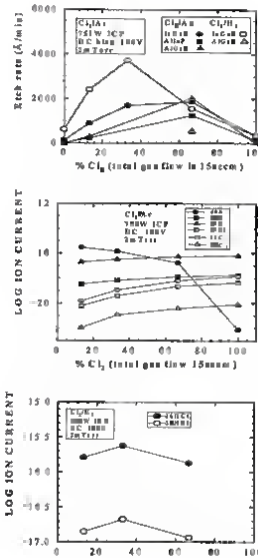

Figure 4-2 Etch rates of InGaP, AlInP and AlGaP (top) or intensities of plasma species from mass spectra (center, bottom) as a function Cl_2 percentage in either Cl_2/Ar or Cl_2/H_2 discharges at fixed pressure (2mTorr), dc bias (-100V) and ICP source power (750W)

Since the volatilities of the etch products for AlGaP should be on average higher than for the In-containing compounds ($InCl_3$ has the lowest vapor pressure), this indicates that the etch rate for AlGaP is at least in part limited by the initial bond breaking that must precede formation of the etch products.

In an ICP system, the ion flux increases as the source power is increased. Figure 4-4 (top) shows that at constant ion energy (dc self-bias is held constant by also increasing the rf power on the chuck from ~70W to 225W as the source power is increased), the increased ion flux at higher source powers leads to an increase in etch rates of all three materials. There are well defined threshold source powers for the onset of etching, indicating that a certain ion flux is required to both break the bonds, and help desorb the resultant etch products. While InGaP showed a very high etch rate (>1μm/min) at high source power (1000W), the more strongly bonded AlGaP and AlInP did not show the same increase in etch rate at high source power. There is an etch selectivity of ~3:1 for InGaP over the other two ternaries at high source powers in this chemistry. Figure 4-4 (bottom) shows the etch yields of three ternary materials as a function of ICP source power. In contrast to the CH_4/H_2-based chemistry, the ion-assisted desorption is more efficient with Cl_2/Ar discharges and thus provides the necessary chemical enhancement to overcome the barrier of desorption of involatile In etch products. Etch yield of InGaP above 750W ICP source power went up rapidly, a good indication of chemical-driven mechanism.

Apart from ion flux, the ion energy, controlled by rf power applied to the chuck position also has a strong influence on etch rates.

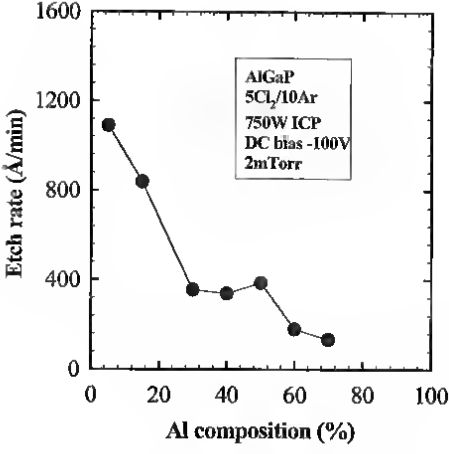

Figure 4-3 Etch rate of AlGaP as a function of Al composition in 2mTorr, -100V dc, 750W ICP, $5Cl_2/10Ar$ discharges.

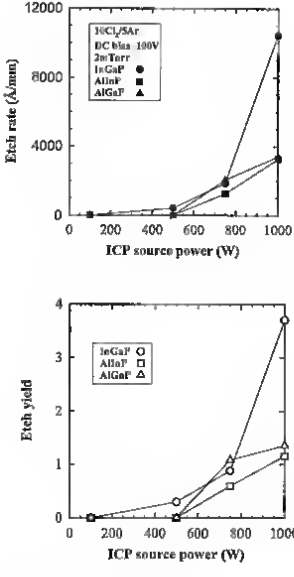

Figure 4-4 Etch rates (top) and etch yields (bottom) of InGaP, AlInP and AlGaP as a function of ICP source power in 2mTorr, -100V dc, $10Cl_2/5Ar$ discharges

Figure 4-5 shows the etch rate dependence on ion energy for all three semiconductors. All materials showed a monotonic increase in etch rates above –35V dc bias, suggesting the presence of the threshold ion energy for the etching to commence. We believe that threshold ion energy is related with the energy barrier of either bond breaking or desorption of etch products. Even under high density plasma conditions in which ion flux is high enough, a certain ion energy is necessary to provide a good chemical enhancement. Only well-controlled combinations of ion flux and ion energy can lead to the ion-neutral synergism. AlInP showed a slower etching compared to other two materials. This might be related with the native oxide, which grows on the surface to form relatively stable Al_2O_3. We did not observe much difference in etching behavior between InGaP and AlInP in ECR reactor, which is equipped with load-lock system, with Cl_2-based chemistry.[51,52] Exposure to the atmosphere for ICP chamber is likely to be sensitive for oxidation of Al-containing materials.

Ion/neutral ratio has a strong effect on the etched surface roughness. As shown in Figure 4-6, Cl_2/Ar discharges produced smooth surface of InGaP after etching in the range of 33~67 % Cl_2 which is consistent with the high etch rate of InGaP. Below the optimized range, the surface became rough due to the preferential sputtering of group V element, phosphorous (P). The Cl_2/H_2 chemistry showed a somewhat different trend. The smoothest surfaces were obtained at 33%, at which the maximum etch rate (~3800Å/min) of InGaP was achieved, and above this composition, the surface was degraded. Surface roughness also depends upon the source power. Figure 4-7 shows AFM surface images of the etched surface of InGaP with $10Cl_2/5Ar$ chemistry at constant dc bias (-100V).

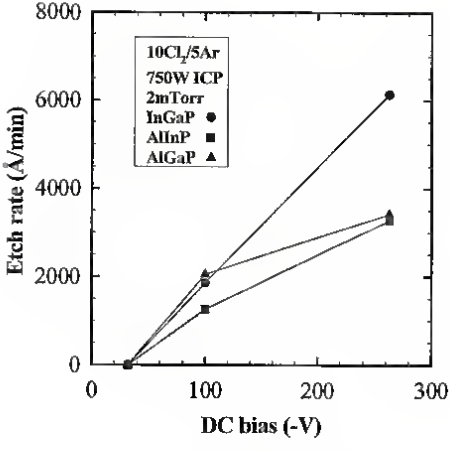

Figure 4-5 Etch rates of three ternary compound semiconductors as a function of dc self bias in 2mTorr, 750W ICP, $10Cl_2/5Ar$ discharges.

RMS roughness value, obtained from Atomic Force Microscopy (AFM), was decreased from 4 1nm to 2 8nm as source power is increased High ion flux available at the high source power enhanced sputter desorption of involatile etch products, leading to the smoother surface with high etch rate AlInP shows a similar behavior to InGaP in terms of surface roughness Figure 4-8 shows surface roughness dependence on ion energy and source power for AlInP Both high ion energy and high ion flux resulted in smooth surface, respectively SEM micrographs for AlInP etched under two different conditions are shown in Figure 4-9 At –100V dc bias, 2mTorr pressure, the surfaces are reasonably good over an optimized range of plasma compositions.

AES surface scans and depth profiles after etching in either Cl_2/Ar or Cl_2/H_2 at the plasma compositions that approximately maximizes etch rate (i.e $10Cl_2$/5Ar, $5Cl_2/10H_2$) are shown in Figure 4-10 and Figure 4-11, respectively There is oxygen present in all cases from the native oxide that grows on the sample during transfer from the etch reactor to the AES analysis chamber, and also carbon from the same exposure to ambient air No chlorine-containing residues were detected in both discharges, indicating no chlorinated layers built up on the surface The surface etched in $10Cl_2$/5Ar discharges revealed no In enrichment at the near surface (~100Å) and there was no sign of phosphorous deficiency The result provided by $5Cl_2/10H_2$ discharges was comparable to the case of Ar addition.

4.2.2. BCl_3 Chemistry

Figure 4-12 shows etch rates of three ternary semiconductors as function of gas composition change in either BCl_3/Ar (top) or BCl_3/H_2 (bottom) discharges at fixed source power (750W) and pressure (2mTorr)

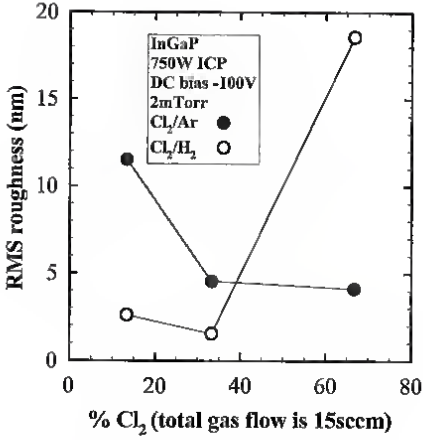

Figure 4-6 RMS surface roughness of InGaP as a function of gas composition in either Cl_2/Ar or Cl_2/H_2 discharges at constant dc bias (-100V) and source power (750W)

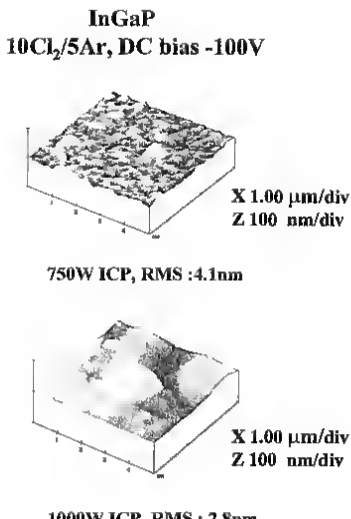

Figure 4-7 AFM scan images of InGaP in 2mTorr, -100V dc $10Cl_2/5Ar$ discharges at either 750W ICP source power (top) or 1000W ICP source power (bottom)

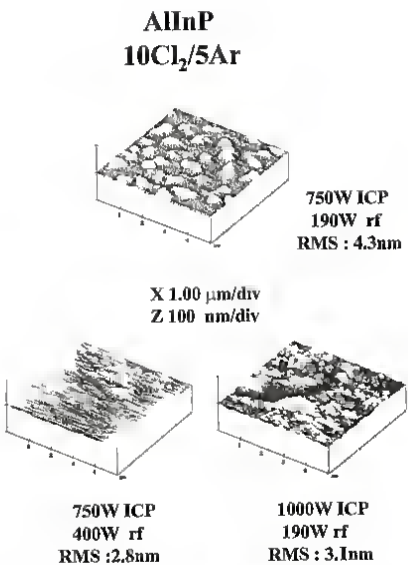

Figure 4-8 AFM scan images of AlInP at the different rf power and source power in $10Cl_2/5Ar$ discharges

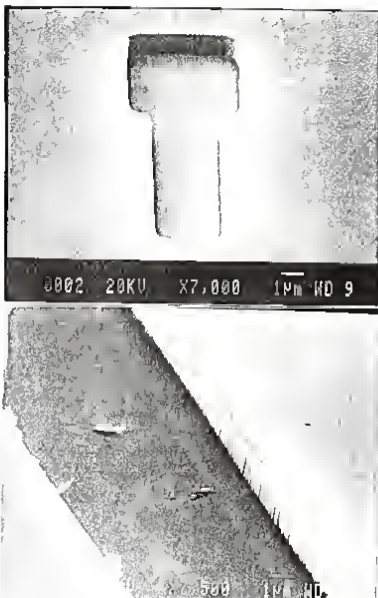

Figure 4-9 SEM micrographs of features etched into AlInP in 2mTorr, 1000W ICP, $10Cl_2/5Ar$ discharges (top) or 2mTorr, 750W ICP, $5Cl_2/10Ar$ discharges (bottom) at constant dc bias (-100V)

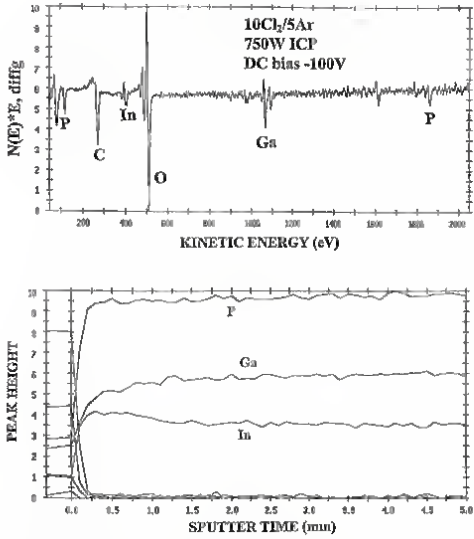

Figure 4-10 AES surface scan (top) and depth profile (bottom) from InGaP after etching in 2mTorr, -100V dc, 750W source power, $10Cl_2/5Ar$ discharges

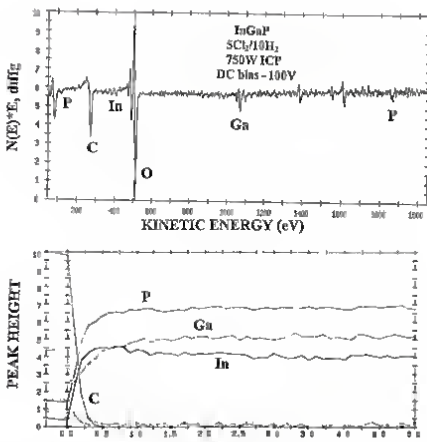

Figure 4.11 AES surface scan (top) and depth profile (bottom) from InGaP after etching in 2mTorr, -100V dc, 750W source power, $5Cl_2/10H_2$ discharges

Two different dc biases were chosen in both discharges for comparison. Etch rates of all three materials peak around 20% BCl_3, which is lower compared to the case of Cl_2 chemistry at –100V dc with Ar addition. AlGaP showed a faster etching than In-based materials at pure BCl_3. However, increasing bias up to –200V led to drastic increase in etch rates for all three semiconductors, indicatioo of a strong chemical enhancement involved. Note that etching proceeded without any suppression until pure BCl_3 at high ion energy (dc –200V), suggesting reactioo-limited, whereas etching is controlled by desorption limited above 20% BCl_3 at low ion energy (dc –100V). BCl_3/H_2 discharges showed a similar behavior. InGaP, AlInP and AlGaP showed much higher etch rates with high ion energy (dc –200V) at the whole range of gas composition. Peak in etch rate for InGaP occurred at 33.3% BCl_3 concentration at low dc bias (-100V), just like the case of Cl_2/H_2 discharges. Higher etch rate for InGaP with BCl_3/H_2 discharges arises from the creation of HCl species in the plasma.

Mass spectra of plasma species in both $5BCl_3/10Ar$ and $5BCl_3/10H_2$ discharges are compared in Figure 4-13, at fixed source power (750W), dc bias (-100V) and pressure (2mTorr). Atomic chlorine components occurred at 35, 36, 37AMU with appearance of Ar components at 20 and 40AMU in BCl_3/Ar combination. With addition of hydrogen in place of Ar, HCl components showed up in the range of 35~38AMU. We suspect that gas phase reaction in the plasma, in which hydrogens were combined with atomic or molecular chlorines creating HCl and Cl radicals, led to the enhanced etch rate for InGaP. The optical emission spectroscopy data is in good agreement with the results obtained from mass spectroscopy.

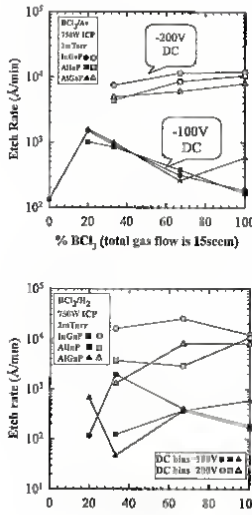

Figure 4-12. Etch rates of InGaP, AlInP and AlGaP as a function of gas composition in either BCl_3/Ar (top) or BCl_3/H_2 (bottom) at the fixed source power (750W) and pressure (2mTorr) with two different dc biases (–100V, –200V)

$5BCl_2/10Ar$ chemistry showed strong chlorine peak at 808.3nm with Ar at 750nm at 750W ICP, -200V dc and 2mTorr, as represented in Figure 4-14 (top) By contrast, $5BCl_2/10H_2$ mixture revealed no chlorine peak, showing only hydrogen at 486 and 656nm at the same condition, as indicated in Figure 4-14 (bottom), which suggests the reaction of chlorine with hydrogen to create HCl. Cl components might be overlapped with those of HCl in the mass spectrum in BCl_2/H_2 discharges but chances are that most chlorines were converted into the HCl, resulting in the disappearance of Cl peak in optical emission spectroscopy

In an ICP tool, source power controls dissociation of gas molecules into ions and reactive neutrals in the plasma Optical emission spectrum (Figure 4-15, top) and peak intensity of chlorine and argon (Figure 4-15, bottom) shows this role of source power to provide radicals Strongest peak for chlorine appeared at 808.3nm in 2mTorr, 1000W ICP, $5BCl_2/10Ar$ discharges at –200V dc bias We normalized the chlorine peak with 750nm Ar as a function of source power Normalized intensity increased steadily up to 1000W source power, a good indication of more radicals available at high source power

Figure 4-16 shows either etch rates (top) or etch yields (bottom) for InGaP, AlInP and AlGaP as a function of source power at the two different ion energies Etch rates of three ternaries increased with source power due to the higher density of neutrals and ions available, as confirmed partly in Figure 4-15 Ion energy had a strong effect on the etching behavior Etch yields of InGaP, AlInP and AlGaP remained at near constant values for the whole range of source power we investigated at –100V dc, suggesting an ion-driven mechanism

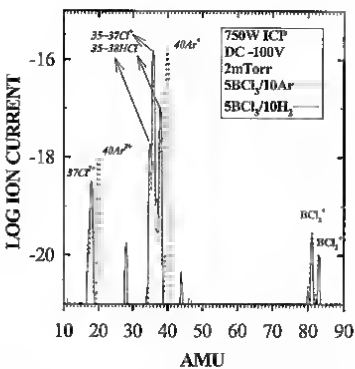

Figure 4-13 Mass spectra of plasma species from both $5BCl_3/10Ar$ and $5BCl_3/10H_2$ discharges at fixed source power (750W), dc bias (-100V) and pressure (2mTorr).

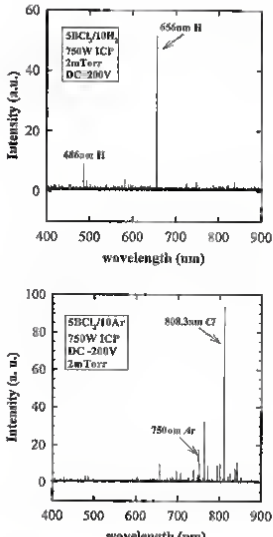

Figure 4-14. Optical emission spectra in either $5BCl_3/10Ar$ or $5BCl_3/10H_2$ discharges at fixed source power (750W), dc bias (200V) and pressure (2mTorr)

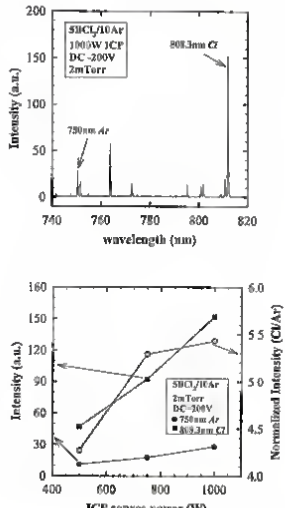

igure 4-15 Optical emission spectra in 2mTorr, 1000W ICP, $5BCl_3/10Ar$ discharges at 200V dc (top) and normalized intensity as a function of source power (bottom)

Increasing dc bias to –200V resulted in much enhanced etch rates of all semiconductors, with InGaP reaching more than 1μm min^{-1}. Etch yields of InGaP and AlInP increased above 750W ICP source power, indicating chemical-driven mechanism.

Since the etching was strongly dependent on ion energy with the BCl_3/Ar chemistry, we investigated etch rates of InGaP, AlInP and AlGaP as a function of dc self bias in 2mTorr, 750W ICP, 5BCl_3/10Ar discharges, as shown in Figure 4-17. Rapid etching of all three materials was obtained above –100V dc self bias, an indication of the presence of a threshold ion energy. Threshold ion energy was reported around –35V dc self bias with Cl_2/Ar chemistry. We believe that this threshold ion energy is related to the activation energy barrier for both desorption of involatile In etch products and bond breaking of strong materials. Since InGaP has the lowest bond strength, it showed the fastest etching once ions get an energy high enough to provide sputter-enhanced desorption of involatile In etch products ($InCl_x$).

Smooth surface morphologies with low RMS roughness values were obtained at optimized ion-to-neutral ratio. As represented in Figure 4-18, increasing BCl_3 percentage from 20% to 33.3% produced improved surfaces of InGaP with RMS roughness value of 5.9nm. Hydrogen addition produced an even better surface with high etch rate (2000Å·min^{-1}). Representative scanning electron micrographs of features etched into InGaP using SiN_x masks are shown in Figure 4-19. Under conditions where etch rate is near maximum at low ion energy (dc –100V), i.e. 5BCl_3/10Ar, 750W source power, 2mTorr, the surface is rough and shows the presence of In droplets (top, left).

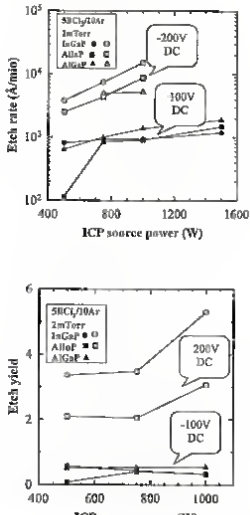

Figure 4-16 Etch rates (top) and etch yields of InGaP, AlInP and AlGaP as a function of ICP source power in 2mTorr, $5BCl_3/10Ar$ discharges at two different ion energies

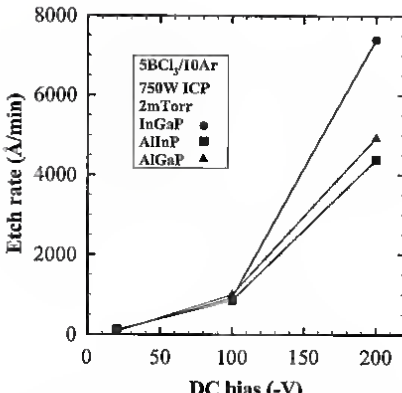

Figure 4-17. Etch rates of InGaP, AlInP and AlGaP as a function of dc self bias in 2mTorr, 750W ICP, $5BCl_3/10Ar$ discharges.

InGaP
750W ICP, DC bias -100V

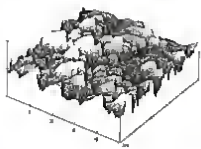

$3BCl_3/12Ar$
RMS : 17.0 nm

X 1.00 μm/div
Z 100 nm/div

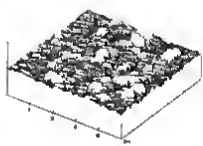

$5BCl_3/10Ar$
RMS : 5.9 nm

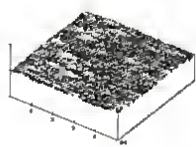

$5BCl_3/10H_2$
RMS : 3.2 nm

Figure 4-18 AFM surface scan images of InGaP in 2mTorr, 750W ICP, -100V dc, BCl_3/Ar or BCl_3/H_2 discharges at the different gas compositions

Enhanced ion-assisted desorption of $InCl_x$ at high ion energy (dc –200V) led to quite smooth surface and anisotropic profiles in 750W ICP, $10BCl_3/5Ar$ discharges (bottom, left and right) $5BCl_3/10H_2$ discharges also provided a comparable surface and profile at –200V dc self bias (top, right) SEM micrographs for AlInP etched under two different conditions are shown in Figure 4-20 At low ion energy (–100V dc), $5BCl_3/10Ar$ discharges produced rough surface and undercut profile (top) On the country, the surface etched at high dc bias of –200V with $10BCl_3/5Ar$ discharges was smooth without any sign of Cl residues on the surface and profile was quite vertical (bottom) Auger Electron Spectroscopy (AES) surface scans from AlInP before and after etching in $5BCl_3/10Ar$ discharges as a function of source power and dc self bias are shown in Figure 4-21 There is oxygen present in all cases from the native oxide during transfer from the etch reactor to the AES analysis chamber, and also carbon from the same exposure to ambient air The sample etched at low ion energy (dc –100V) has a high coverage of chlorine-containing residues, consistent with rough surface and low etch rate Increasing ion flux reduced the concentration of the chlorinated residues, which is most likely related to the improved sputtering efficiency at higher source power High ion energy (dc –200V) led to drastic reduction of Cl peak on the surface, which is in good agreement with fast etching at this condition

4.2.3. $Cl_2/BCl_3/Ar$ Chemistry

Figure 4-22 shows optical emission spectra from $Cl_2/BCl_3/5Ar$ discharges as a function of Cl_2/BCl_3 composition at fixed source power (500W), dc bias (-150V) and pressure (2mTorr) Strong peaks occurred at 413nm for Cl^* and 837.5nm for Cl

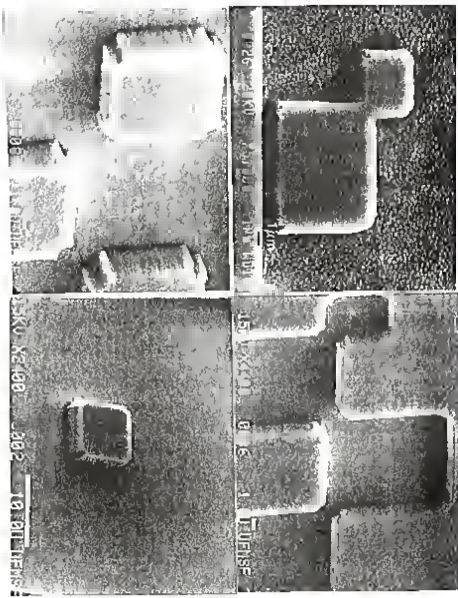

Figure 4 19 SEM micrographs of features etched into InGaP in different ion energies and gas compositions

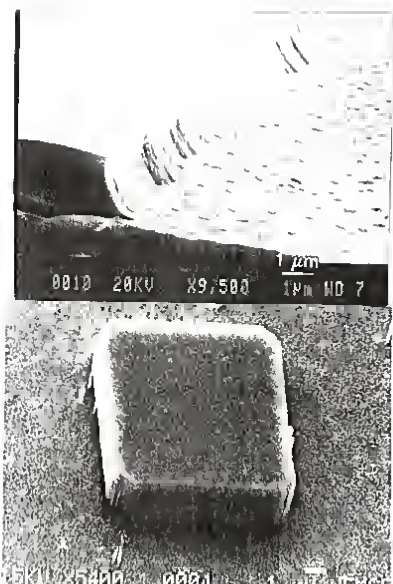

Figure 4-20 SEM micrographs for AlInP etched in either -100V dc $SBCl_3/10Ar$ discharges (top) or -200V dc $10BCl_3/5Ar$ discharges (bottom) at fixed source power (750W) and process pressure (2mTorr)

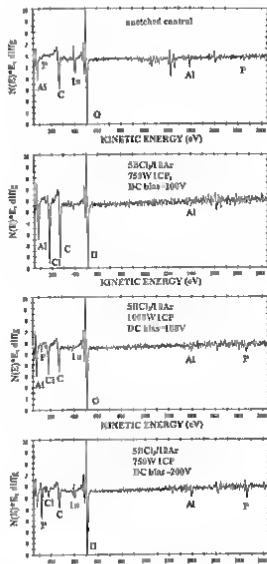

Figure 4-21 AES surface scans from AlInF before and after etching in 2mTorr, $5BCl_3/10Ar$ discharges at the different source powers and ion energies

First thing to note is that all peaks corresponding to Cl showed maximum intensity at $32Cl_2/8BCl_3/5Ar$ composition. It is believed that Cl_2 can produce more Cl neutrals than BCl_3. One more additional feature is that adding a small amount of BCl_3 to Cl_2 creates many more neutrals than either pure Cl_2 or pure BCl_3. Secondly, BCl_3 is more sensitive to the creation of molecular species than Cl_2. As shown in Figure 4-22 (top), molecular continua in the spectrum becomes much more dominant as BCl_3 concentration is increased. We have used mass spectrometry to identify the plasma species available. As shown in Figure 4-23, heavy molecular BCl_x species (81, 83, and 85AMU) were detected from BCl_3 relative to Cl_2 ($70Cl_2$, $72Cl_2$, and $74Cl_2$). Figure 4-24 shows etch rates of InGaP and AlInP (top), and normalized optical emission intensity (bottom) as a function of Cl_2/BCl_3 composition change at fixed source power (750W), dc bias (-150V) and pressure (2mTorr). Etch rates of the two semiconductors are increased in the range from 40% Cl_2 to 80% Cl_2 and then dropped to minimum at pure Cl_2, which is in good agreement with the optical emission intensities. We can divide etching mechanism into two regions at these conditions. Etching is controlled by neutral species in the range from 40% to 100% Cl_2, an indication of reaction-limited conditions, whereas heavy BCl or BCl_2 molecular ions made contribution to the increase of etch rates in the range of 0~40% Cl_2, a sign of desorption-limited etching. It is likely that molecular continua from optical emission arised from BCl or BCl_2 molecular species.

Figure 4-25 shows the dependence of InGaP and AlInP etch rates on source power in 2mTorr, $32Cl_2/8BCl_3/5Ar$ discharges at constant dc bias of –150V. InGaP showed an increase in its etch rate up to 1800Å·min^{-1} at 1000W source power due to the abundant ion flux at high source power.

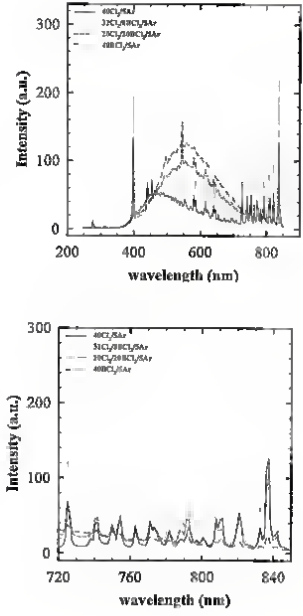

Figure 4-22 Optical emission spectra from 2mTorr, $Cl_2/BCl_3/5Ar$ discharges as a function of Cl_2/BCl_3 composition at fixed source power (500W) and dc bias (150V)

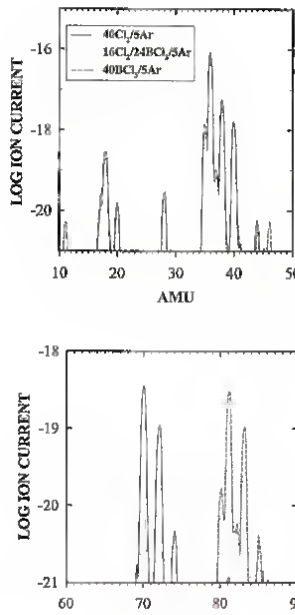

Figure 4-23 Mass spectra from 2mTorr, $Cl_2/BCl_3/5Ar$ discharges as a function of Cl_2/BCl_3 composition at fixed source power (750W) and dc bias (-150V)

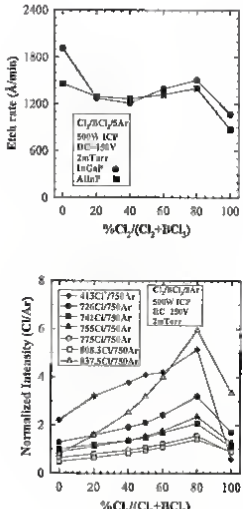

Figure 4-24 Etch rates of InGaP and AlInP (top), and normalized intensity of optical emission spectra as a function of gas composition in 2mTorr, -150V dc, 500W ICP, $Cl_2/BCl_3/5Ar$ discharges

AlInP showed a similar behavior to InGaP, suggesting the same etching mechanism at these conditions

Ion energy is likely to be most dominant factor for the etching of InGaP and AlInP with $Cl_2/BCl_3/5Ar$ chemistry As indicated in Figure 4-26 (top), etch rates of InGaP increased monotonically up to ~6000Å min^{-1} at –400V dc bias On the contrary, AlInP showed somewhat different trends, with a rapid increase in its etch rate above –300V dc bias. Selectivity of AlInP over InGaP was around 2 at high dc bias (-400V) Selectivity for AlInP over InGaP has never been previously reported This might be related to the oxidation breakthrough step during the etching for AlInP in an ICP tool, equipped with loadlock system Figure 4-26 (bottom) showed normalized optical emission intensity as a function of dc self bias in 2mTorr, 500W ICP, $32Cl_2/8BCl_3/5Ar$ discharges Intensities of all species increased from –50V to –150V dc and then remained constant above –150V We believe that capacitively coupling made a small contribution to the production of species in the range –50V—150V dc, which did not have much effect on etch rate since ion energy was a dominant factor for the etching.

Figure 4-27 shows etch rates of the two semiconductors (top) and normalized intensities of mass spectra (bottom) as a function of process pressure Pressure controls the ion-to-neutral ratio The general belief is that the chemical component of the etching becomes dominant as pressure is increased Intensity corresponding to $37Cl^+$ decreased relative to atomic chlorines (35Cl, 36Cl) with pressure, indicating neutral species become dominant over the ionic component at high pressure. Additionally, Cl_2 and BCl_3 molecular species are increasing above 2mTorr, possibly due to the recombination of atomic species

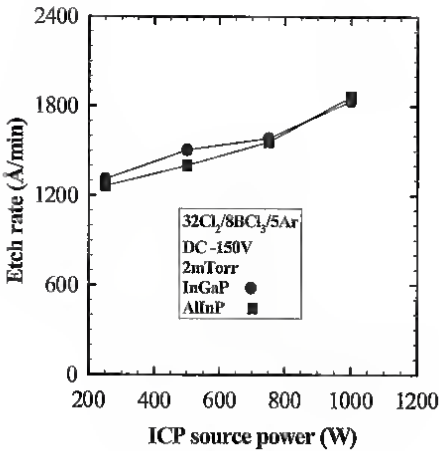

Figure 4-25 Etch rates of InGaP and AlInP as a function of source power in 2mTorr, $32Cl_2/8BCl_3/5Ar$ discharges at −150V dc bias.

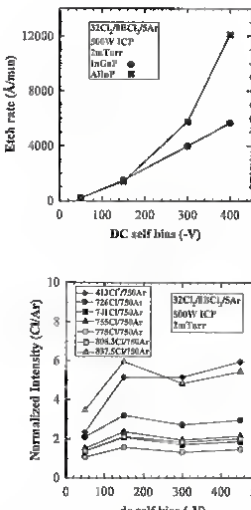

Figure 4-26 Etch rates of InGaP and AlInP (top), and normalized intensities from optical emission spectra (bottom) as a function of dc self bias in 2mTorr, 500W ICP, $32Cl_2/8BCl_3/5Ar$ discharges.

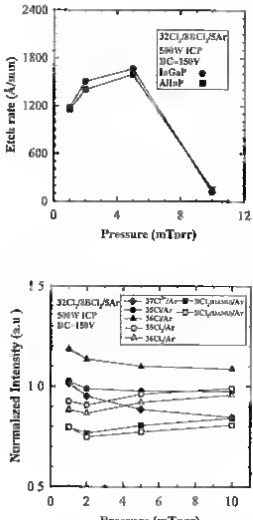

Figure 4-27. Etch rate of InGaP and AlInP (top), and Normalized intensities from mass spectra (bottom) as a function of process pressure in $32Cl_2/8BCl_3/5Ar$ discharges at fixed source power (750W) and dc self bias (-150V)

The maximum etch rates of InGaP and AlInP were achieved at the pressure of 5mTorr, which provided optimized ion-to-neutral ratio The suppression of etching above 5mTorr should be related to the shortage of either ions or etchants

Surface roughness of InGaP etched in 2mTorr, -150V dc, $32Cl_2/8BCl_3/5Ar$ discharges showed a strong dependence on ICP source power As shown in Figure 4-28, root-mean square (RMS) of InGaP, measured by Atomic Force Microscopy (AFM), dropped to 3 2nm at 750W source power, due to the efficient sputter desorption of In etch products ($InCl_x$) However, increasing source power up to 1000W degraded the etched surface, arising from the preferential sputtering of phosphorous (P) Figure 4-29 shows etched surface of AlInP as a function of source power and ion energy in 2mTorr, $32Cl_2/8BCl_3/5Ar$ discharges. Smooth surface, with low RMS value (2 1nm), was obtained at the moderate source power (500W) and ion energy (-150V dc) The surface becomes roughened at high source power (1000W) and ion energy (-400V dc), probably due to its non-stoichiometry surface Surface morphologies of InGaP and AlInP etched at different source power and ion energy are shown in Figure 4 30 The profiles of InGaP (top, left) and AlInP (top, right) were almost anisotropic at moderate source power (750W) and ion energy (-150V dc) High dc bias (400V) resulted in smooth surface of InGaP (bottom, right) without the presence of In droplets, which indicates the equitate removal of different etch products Using photoresist as a mask led to the rough sidewalls, (striations transferred from photoresist, bottom, left), while SiN_x masks degraded themselves upon exposure to the plasma (top, left and right, or bottom, right)

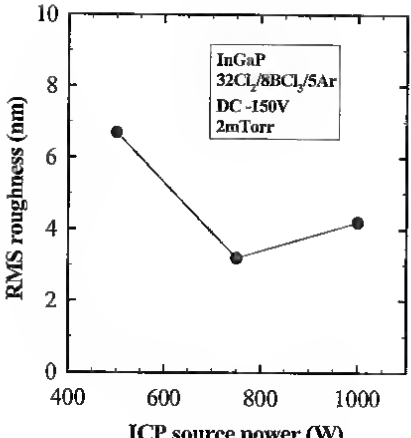

Figure 4-28 RMS roughness of InGaP after etching in 2mTorr, -150V dc, $32Cl_2/8BCl_3/5Ar$ discharges as a function of ICP source power.

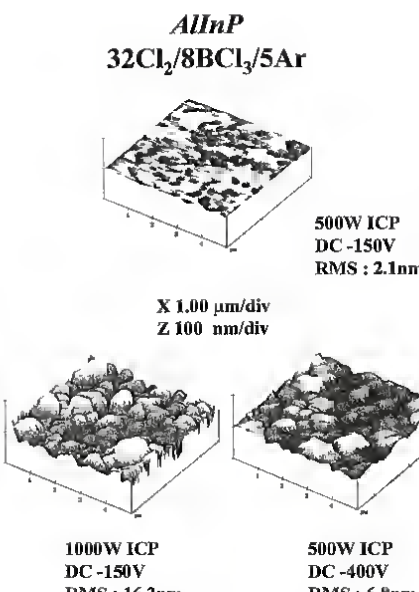

Figure 4-29. AFM surface scan images of AlInP etched in 2mTorr, $32Cl_2/8BCl_3/5Ar$ discharges at the different source power and ion energy.

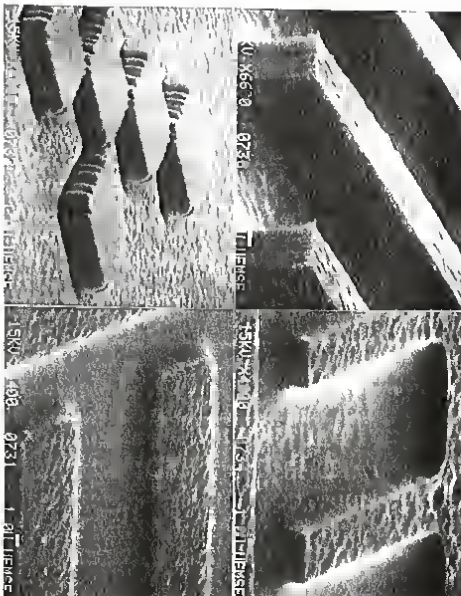

Figure 4-30 SEM micrographs of features etched into InGaP (top, left or bottom, left and right) and AlInP (top, right) with 750W (top) or 500W (bottom) ICP and –150V dc (top),-300V dc (bottom, left) or –400V dc (bottom, right) in $32Cl_2/8BCl_3/5Ar$ discharges. The photoresist mask (bottom, left) has been removed and SiN_x masks are still in place (top, left and right, and bottom, right).

CHAPTER 5
INDUCTIVELY COUPLED PLASMA ETCHING BASED ON NEW PLASMA CHEMISTRIES: BI_3 AND BBr_3

5.1. Materials and Methods

BI_3 is a solid with a melting point of 44°C, while BBr_3 is a liquid with a boiling point of 91.2°C. Approximately 50g of each material was placed in a quartz container within a stainless steel vacuum vessel that was heated to ~45°C to enhance the respective vapor pressures. The vapor was allowed to enter the reactor chamber through a Cl_2-compatible mass flow controller. Maximum flow rates of 5 and 10 standard cubic per minute (sccm) were obtained for BI_3 and BBr_3, respectively, and the total flow rate was typically held at 10sccm by adding in Ar.

Etch rates were obtained from stylus profilometry measurements, while surface morphology was examined by atomic force microscopy (AFM) performed in the tapping mode, and scanning electron microscopy (SEM).

5.2. Results and Discussion

Both BI_3 and BBr_3 were found to be readily dissociated in the ICP source, producing blue-violet discharges. Figure 5-1 shows an optical emission spectrum of pure BI_3 discharges in this wavelength range, revealing a large number of atomic transitions. Figure 5-2 shows etch rates (top) and etch yields (bottom) for the three ternary alloys in $4BI_3/6Ar$ and $4BBr_3/6Ar$ discharges (750W source power, 5mTorr) as a function of dc

chuck bias. There are several key features of the data. First, the etch rates for all three alloys are much higher in BI_3/Ar. Second, the threshold biases for the onset of etching are significantly lower for BI_3 than BBr_3, indicating the etch products are more volatile and require less ion-assistance for desorption. Third, the etch yields with BI_3 are linearly dependent on dc bias, which indicates that the etching is still desorption-limited. For BBr_3 etching of InGaP, the rate decreases at high biases, partly due to removal of the active bromine species by sputtering before they can react with the semiconductor surface.

Figure 5-3 shows etch rates for the three ternary alloys as a function of discharge composition in either 150W rf, BI_3/Ar (top) or 350W rf BBr_3/Ar (center) at fixed source power (750W) and pressure (5mTorr). Note that the dc self chuck bias decreases as BI_3 content increases, suggesting that BI_3 is readily ionized than Ar since dc bias decreases with increasing ion density in the plasma. By contrast, dc bias increases with BBr_3 percentage, which indicates that BBr_3 is more difficult to ionize than Ar. For both plasma chemistries, the etch rate of AlInP is almost independent of discharge composition, whereas that of InGaP increases almost monotonically with boron halide content. In developing device fabrication processes it is necessary to have wet and dry etches that are highly selective for one material over another. There has been little work on selective dry etches for the InGaP/AlInP system. The bottom of Figure 5-3 shows the etch selectivity of InGaP over AlInP as a function of plasma composition for both mixtures. These values are the highest reported for InGaP/AlInP and are easily high enough for device processing schemes. It is well established that InI_x etch products are quite volatile, as are PI_3 species.[34]

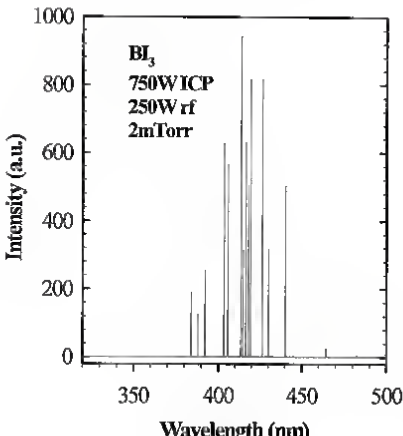

Figure 5-1. Optical emission spectrum from BI_3 discharge

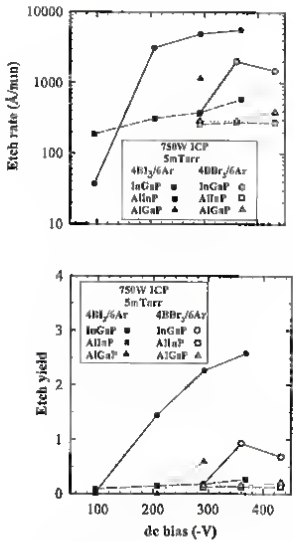

Figure 5-2 Etch rates (top) and etch yields (bottom) for InGaP, AlInP and AlGaP in 750W source power, 5mTorr discharges of $4Br_2/6Ar$ or $4BBr_3/6Ar$ discharges as a function of chuck dc bias.

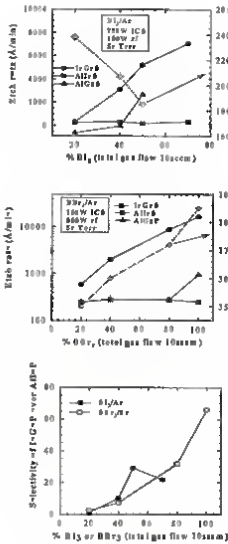

Figure 5-3. Etch rates of InGaP, AlInP and AlGaP in (top) BI_3/Ar discharges (750W source power, 150W rf chuck power) as a function of plasma composition, (center) BBr_3/Ar discharges (750W source power, 350W rf chuck power) as a function of plasma composition, or (bottom) etch selectivity of InGaP over AlInP under these conditions

In BI_3 etching therefore, the etch selectivity for InGaP over AlInP arises from the relatively involatile AlI_x products Similar reasoning applies to the BBr_3 plasma chemistries For AlGaP we observed some deposition at low BI_3 contents, and a practical, controllable rate of ~3000Å min^{-1} at a 50% composition (Figure 5-3, top).

One of the advantages of high density plasma sources is the ability to increase ion density at moderate ion energies Figure 5-4 shows the dependence of alloy etch rate on ICP source power for fixed rf chuck power (150W) and plasma composition ($4BI_3/6Ar$) Note that as source power increases the dc chuck bias decreases due to the higher ion density Under these conditions only InGaP shows a significant etch rate, with a relatively high etch yield (~1 5) at 750W source power Similar data is shown in Figure 5-5 for BBr_3/Ar discharges Once again the chuck self bias decreases as the source power increases, and only InGaP shows a high etch rate and corresponding etch yield.

Since both plasma chemistries are effective for etching InGaP, we focused on the quality of the etched surface morphology for this material Figure 5-6 shows some representative AFM scans. We found that the root-mean square (RMS) roughness decreased with both BI_3 content and rf chuck power Note that increasing the BI_3 percentage from 40 to 50 at fixed rf chuck power produces slightly better surfaces than that of an unetched control sample (RMS value 1 1nm for the latter) A smooth surface almost always indicates that the etch products for In, Ga and P are being removed at essentially equal rates

Basically similar trends were observed for BBr_3 etching of InGaP Figure 5-7 shows some representative AFM scans for different plasma compositions at fixed source power and rf chuck power

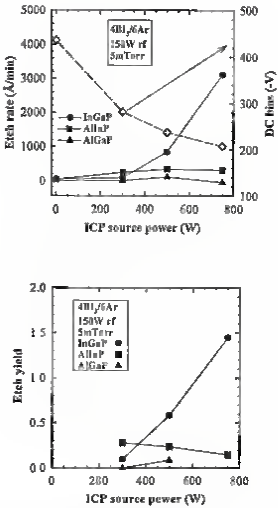

Figure 5-4 Etch rates (top) and etch yields (bottom) for InGaP, AlInP and AlGaP in $4BI_3/6Ar$, 150W rf power, 5mTorr discharges as a function of ICP source power

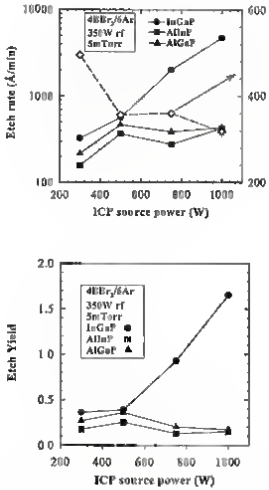

Figure 5-5 Etch rates (top) and etch yields (bottom) for InGaP, AlInP and AlGaP in $4BBr_3/6Ar$, 350W rf power, 5mTorr discharges as a function of ICP source power

Note again that the surface becomes smoother as BBr_3 percentage increases. For both BBr_3 and BI_3 we observed there was no incubation time for the onset of etching, indicating that these gases efficiently remove the native oxide on InGaP, similar to the case of BCl_3.

The etched features were anisotropic under all the conditions we investigated. Figure 5-8 shows some typical SEM micrographs of features etched into InGaP with BBr_3 and BI_3 discharges at different rf chuck powers and plasma compositions. The sidewalls are smooth and vertical, with the etched surface morphologies also being quite good.

Figure 5-9 shows a surface scan (top) and depth profile (bottom) from AlInP after etching in $8BBr_3/2Ar$ discharges at fixed source power (750W) and rf chuck power (350W). The surface etched with this chemistry revealed Al-enrichment at the near surface region (~100Å) leading to the oxidation upon exposure to the atmosphere after etching. This indicates the existence of involatile Al etch product on the surface, which is the source of low etch rate for AlInP.

One of the key considerations in evaluating a plasma chemistry is selectivity with respect to common masking materials. Figure 5-10 (top) shows the etch selectivity for InGaP over plasma enhanced chemical vapor deposited SiO_2 and SiN_x as a function of ICP source power in BBr_3/Ar discharges (350W chuck power, 5mTorr). The selectivities basically increase as the source power increases because the etch rate of InGaP increases rapidly under these conditions. The values obtained at high source powers (8:10) are acceptable for device processing and quite high for etching under high density conditions.

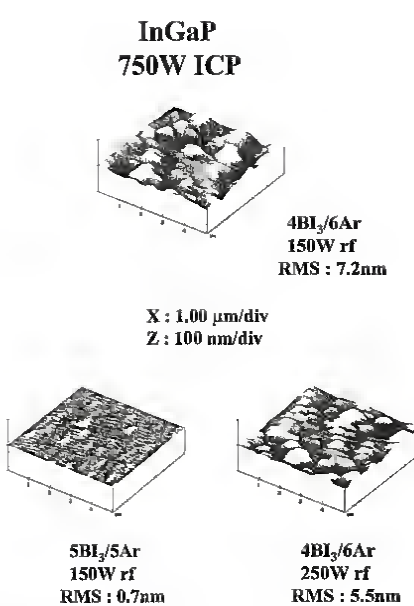

Figure 5-6 AFM scans from InGaP etched in 750W source power, BI_3/Ar discharges with different compositions and rf powers

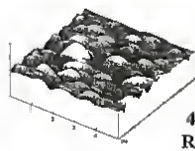

Figure 5.7. AFM scans from InGaP etched in 750W source power, 350W rf power BBr_3/Ar discharges with different compositions.

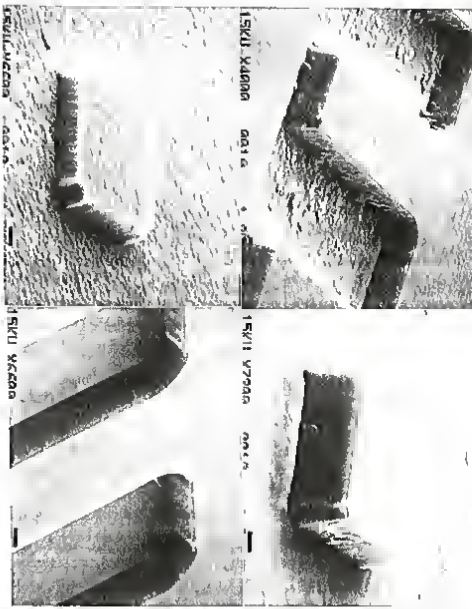

Figure 5-8 SEM micrographs of features etched into InGaP using 750W source power discharges of (top left) $2BI_3/8Ar$ 250W rf power, (top right) $4BI_3/6Ar$, 150W rf power, (bottom left) $8BBr_3/2Ar$, 350W rf power and (bottom right) $10BBr_3$, 350W rf power The SiN_x masks are still in place in all cases

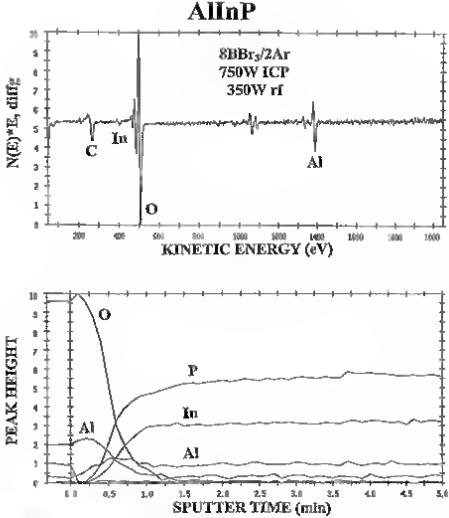

Figure 5.9 AES surface scan (top) and depth profile (bottom) from AlInP after etching in 5mTorr, $8BBr_3/2Ar$ discharges at fixed source power (750W) and rf chuck power (350W)

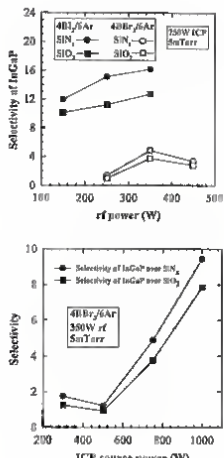

Figure 5-10 Etch selectivities of InGaP over SiO_2 and SiN_x in (top) $4BBr_3/6Ar$ discharges, 350W rf power, 5mTorr, as a function of ICP source power, and (bottom) in $4BI_3/6Ar$ or $4BBr_3/6Ar$, 750W source power, 5mTorr discharges, as a function of rf power

Even higher values were obtained with BI_3/Ar discharges. Figure 5-10 (bottom) shows a comparison of selectivities obtained for InGaP over SiO_2 and SiN_x in the two chemistries, as a function of rf chuck power. Note that the selectivities with BI_3/Ar actually increase with chuck power because the etch rate of InGaP rises faster than that of the dielectrics

CHAPTER 6
ELECTRON CYCLROTRON RESONANCE PLASMA ETCHING BASED ON ICl AND IBr

6.1. Results and Discussion

Figure 6-1 shows the semiconductor etch rates in 1.5mTorr, 1000W ECR, 150W rf discharges of ICl/Ar and IBr/Ar, as a function of the gas compositions measured by flow rate. The rates increase up to 50% ICl or IBr and are basically constant thereafter. The slight reduction in rates for pure ICl or IBr discharges may be due to a reduced ion-assisted sputtering efficiency for the etch products. Note that the rates are much faster for ICl compared to IBr, as expected from the volatilities of their resulting etch products. At 1000W microwave power the rates with ICl/Ar are similar to those achieved in our system with Cl/Ar for the same pressure, gas compositions and rf power.[31]

One of the major advantages with these new gases is shown in Figure 6-2. For InGaP and AlInP the etch rates are essentially independent of microwave power in the range 400-1000W. At 0W microwave (i.e. RIE conditions) the etch rates were only a few hundred angstroms per minute, but the bond strengths of the I-Cl and I-Br are sufficiently low that 400W of microwave power efficiently dissociates the molecules, producing active iodine and chlorine neutral atoms. The ion density at 400W also appears sufficient to efficiently desorb the etch products. AlGaP has a higher average bond strength than the other two materials, as mentioned in the previous chapters and the increase in etch rate at

higher microwave powers may be due to the need for a higher ion density to assist in bond breaking and/or etch product desorption

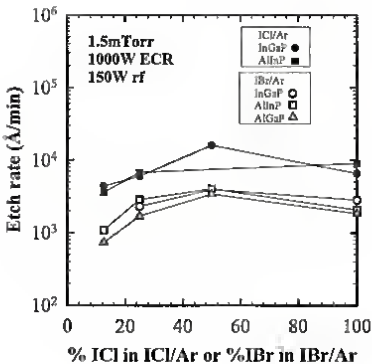

Figure 6-1. Etch rates of ternary alloys as a function of plasma composition in ICl/Ar or IBr/Ar discharges (1000W microwave power, 150W rf power, 1.5mTorr)

As mentioned earlier we have found that at microwave powers of 400-600W, photoresist masks hold up well to plasma exposure with little distortion of their original geometries [52] However, at 1000W there is generally reticulation of the resist after even a short (~1min) exposure For ICl/Ar, etch rates in excess of 1 μm/min are achieved even at 400W ECR source power, which are approximately a factor of five faster than Cl_2/Ar under the same conditions in our reactor [53]

The dependence of semiconductor etch rates on rf chuck power at fixed microwave power and pressure is shown in Figure 6-3 There is a general increase in rate as the average ion energy increases and produces more efficient etch product desorption At 250W rf the ICl/Ar etch rates for InGaP (2 2μm/min) and AlInP (1 7μm/min) are the fastest we have achieved for any plasma chemistry (Cl_2/Ar, Cl_2/H_2, Cl_2/N_2, BCl_3/Ar and CH_4/H_2/Ar)

Typical AFM scans of ICl/Ar etched surfaces are shown in Figure 6-4 At a plasma composition of 4ICl/4Ar, 150W of rf power and 1 5mTorr pressure, higher microwave powers always produced rougher surfaces. For InGaP etched at 600W, the root-mean-square (RMS) roughness measured over a 5×5 μm^2 area was 7 5nm for an etch depth of 1 7μm An unetched control sample had typical RMS values of 1-1 6nm. The sample etched at 1000W microwave power, with a comparable etch depth of 1 6μm, had an RMS roughness of 9 9nm, and shows the spiky surface typical of those that have preferentially lost P A similar result was obtained for AlInP, with the RMS value increasing from 4 9nm at 800W microwave and 150W rf, to 27nm at 1000W microwave and 250W rf (lower part of Figure 6-4)

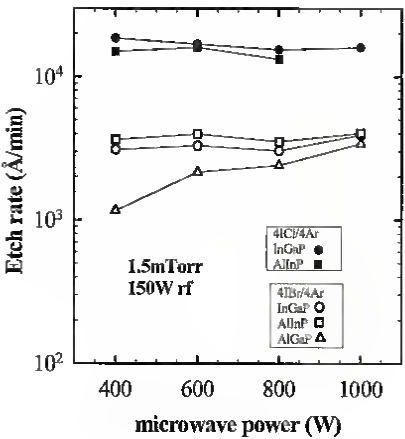

Figure 6-2 Etch rates of ternary alloys as a function of microwave power in 4ICl/4Ar or 4IBr/4Ar discharges (150W rf power, 1.5mTorr)

AFM scans from AlInP etched in 1000W microwave, 150W rf IBr/Ar discharges are shown in Figure 6-5 for different IBr to-Ar ratios The surface morphology is a strong function of the plasma composition. RMS values for both AlInP and InGaP as a function of IBr percentage are shown in Figure 6-6 For InGaP the IBr flow must be kept to low values to achieve acceptable morphologies, while the surfaces for AlInP are best at either high or low IBr percentages At intermediate plasma composition the morphology is quite rough, with the appearance of bullocks This might be due to residual $InBr_3$, which is not particularly volatile, whereas with pure IBr the absence of Ar ions reduces the removal rate of Ga and P etch products and leaves a somewhat better morphology.

An AES surface scan of AlInP after a 8IBr, 1000W ECR power, 150W rf etch is shown in Figure 6-7 The C and O come from exposure of the sample to atmosphere in transferring to the AES chamber The small Si signal appears to result from sputtering or redeposition from the Si carrier wafer There is no detectable Br on the surface, and there is no change in stoichiometry relative to the unetched control sample.

Figure 6-8 shows SEM micrographs of features etched into InGaP (top) or AlInP (bottom) with a 4IBr/4Ar, 750W ECR power, 150W rf, 1 5mTorr discharge. The morphologies are quite good for both materials, although the sidewalls are not completely vertical Smooth surfaces were also achieved with ICl/Ar - Figure 6-9 shows SEM micrographs of features etched into InGaP (top) or AlInP (bottom) with 4ICl/4Ar, 1000W ECR power, 250W rf, 1 5mTorr discharges It is noticeable that the photoresist mask failed at several regions during this etch and thus our earlier discussion concerning the benefits of lower microwave powers.

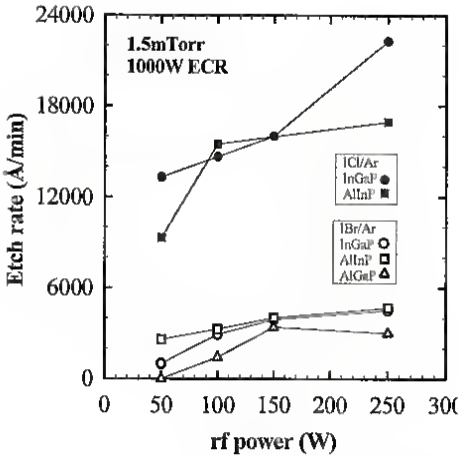

Figure 6-3. Etch rates of ternary alloys as a function of rf power in 4ICl/4Ar or 4IBr/4Ar discharges (1000W microwave power, 1.5mTorr).

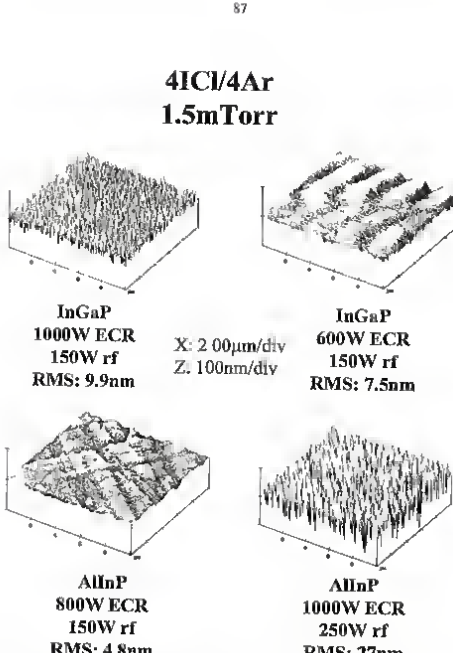

Figure 6-4 AFM scans of InGaP (top) or AlInP (bottom) after etching in 4ICl/4Ar, 1.5mTorr discharges at 1000W microwave power, 150W rf (top, left), 600W microwave, 150W rf (top, right), 800W microwave, 150W rf (bottom, left), or 1000W microwave, 250W rf (bottom, right).

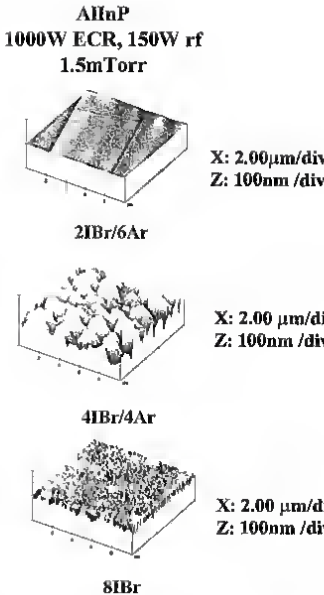

Figure 6-5. AFM scans of AlInP after etching in 1000W microwave, 150W rf, 1.5mTorr discharges of 2IBr/6Ar (top), 4IBr/4Ar (center), or 8IBr (bottom)

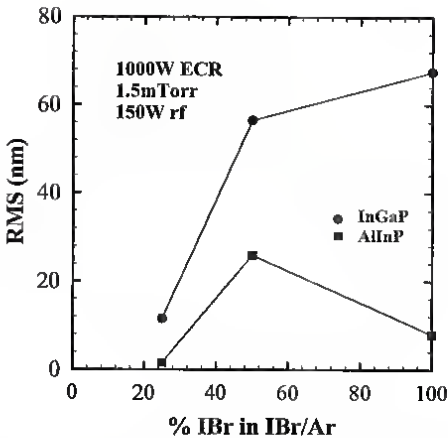

Figure 6-6 RMS surface roughness of InGaP and AlInP samples after etching in 1000W microwave, 150W rf, 1.5mTorr IBr/Ar discharges as a function of plasma composition

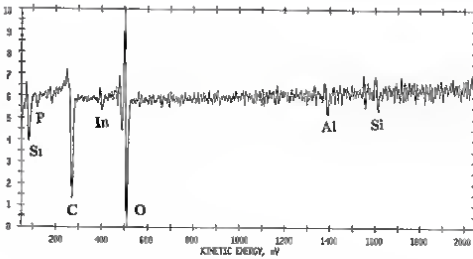

Figure 6-7 AES surface scan of AlInP after etching in a 1000W microwave, 150W rf, 1.5mTorr discharges of SiBr

We have previously found that the etch rate of $Al_xGa_{1-x}P$ alloys is fairly constant for $x = 0 \rightarrow 0.6$, and decreases thereafter in Cl_2 and BCl_3 plasma chemistries [1]. Similar results were obtained with IBr/Ar, as shown in Figure 5-10. Thus Al-rich AlGaP alloys are good candidates as etch stop layers in device structures requiring close control of etch depth, provided of course that they do not interfere with carrier transport within the device.

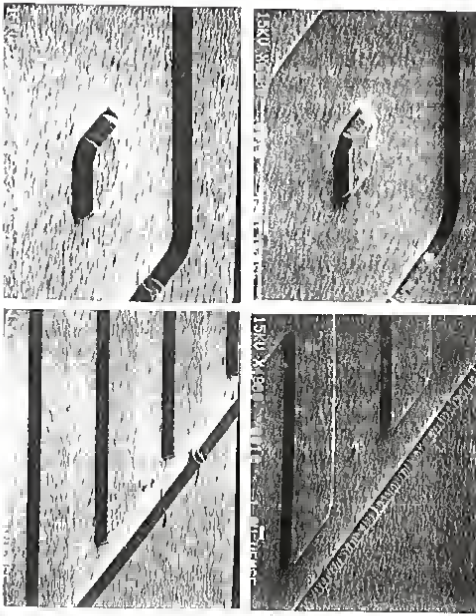

Figure 6 8 SEM micrographs of features etched into InGaP (top) or AlInP (bottom) with a 750W microwave, 150W rf, 1 5mTorr discharges of 4IBr/4Ar The photoresist mask has been removed

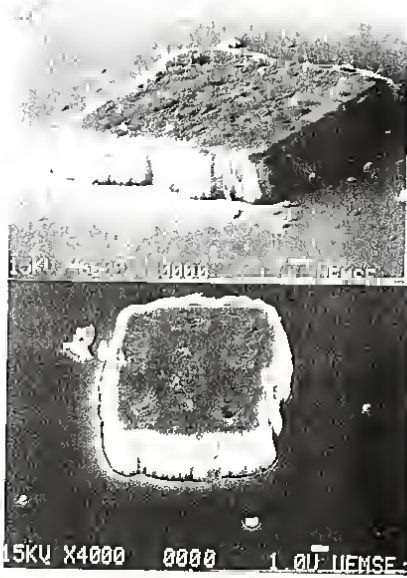

Figure 6-9 SEM micrographs of features etched into InGaP (top) or AlInP (bottom) with 1000W microwave, 250W rf, 1 5mTorr discharges of 4ICl/4Ar The photoresist masks have been removed

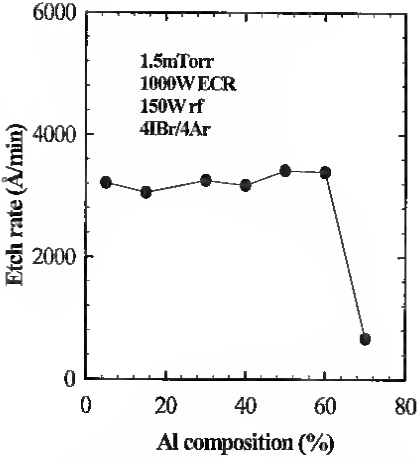

Figure 6-10 Etch rates of $Al_xGa_{1-x}P$ alloys as a function of Al compositions in 1000W microwave, 150W rf, 1.5mTorr discharges of 4IBr/4Ar

CHAPTER 7
SUMMARY

We have compared several gas chemistries based on $CH_4/H_2/Ar$, Cl_2/Ar, Cl_2/H_2, BCl_3/Ar, BCl_3/H_2, Bl_3/Ar, BBr_3/Ar, ICl/Ar and IBr/Ar in Inductively Coupled Plasma (ICP) and Electron Cyclotron Resonance (ECR) tools. The characteristics for each are summarized in Table 7-1. CH_4/H_2-based chemistry combined with high density plasma tools (ICP, ECR) did not provide good results. Etch rates of all three materials (InGaP, AlInP, AlGaP) were low without ion-neutral synergism. Etched features did not show anisotropic profiles, and etched surfaces were rather rough and non-stoichiometric with In-enrichment at the near surface (~100Å). Most of all, etching with this chemistry proceeded through an ion-driven mechanism.

Cl_2-based chemistries provided better results than $CH_4/H_2/Ar$ in the ICP tool, as a whole. Cl_2/Ar discharges showed a strong chemical enhancement for the etching of InGaP at high source power (1000W) with high etch yield (~4). The surface etched with this chemistry revealed no chlorine residues without any indication of phosphorous (P) deficiency. Hydrogen addition to Cl_2 produced new plasma species (HCl) as confirmed by Optical Emission Spectroscopy (OES) and Mass Spectrometry, with higher etch rate of InGaP and stoichiometric surface. BCl_3/Ar discharges showed a strong dependence of ion energy for the etching of all three ternary compounds, with well-defined threshold ion energy (~-20V dc).

Table 7-1 Typical results for the etching of InGaAlP ternary compounds in High Density Plasma tools.

Gas Chemistry (etch tool)	Comments	Typical rates
$5CH_4/15H_2/10Ar$ (ECR, ICP)	• no ion neutral synergism (ion-driven mechanism) • low etch rate • rough surface with sloped side wall • non-stoichiometric surface (In enrichment)	~1500Å/min for InGaP <1000Å/for AlInP, AlGaP
Cl_2/Ar, Cl_2/H_2 (ICP)	• ion neutral synergism • threshold ion energy • smooth surface (<4nm RMS for InGaP) • no In-enrichment, no P deficiency at the near surface • HCl creation with H_2 (higher etch rate, smoother surface)	>1μm/min for InGaP >3000Å/min for AlInP, AlGaP
BCl_3/Ar, BCl_3/H_2 (ICP)	• ion-driven at low ion energy (rough surface, high coverage of chlorine residues) • chemical-driven at high ion energy (smooth surface) • threshold ion energy • BCl_3/H_2 produced HCl with faster etching	>1μm/min for InGaP <5000Å/min for AlInP, AlGaP
$Cl_2/BCl_3/Ar$ (ICP)	• Selectivity of AlInP over InGaP (~2) at high ion energy • smooth surface with anisotropic profile	~6000Å/min for InGaP ~1.2μm/min for AlInP
Br_2/Ar, BBr_3/Ar (ICP)	• higher etch rates with Br_2/Ar • high selectivity of InGaP/AlInP • chemical enhancement only for InGaP • involatile etch products of Al	0.7~1.0μm/min for InGaP <500Å/min for AlInP, AlGaP
ICl, IBr (ECR)	• fastest etching with ICl • etching not dependent on μwave in 400~1000W	2.0μm/min for InGaP with ICl 1.6μm/min for AlInP with ICl <4000Å/min for InGaP, AlInP, AlGaP with IBr

The etching mechanism changed from ion-driven at low ion energy (-100V dc) to chemical-driven at high ion energy (-200V dc). Surface morphologies improved with ion energy with less chlorine residues on the surface at high ion energy. The combination of Cl_2 with BCl_3 resulted in high selectivity of AlInP over InGaP at high ion energy.

Iodine based chemistries provided high etch rates for InGaP, as predicted from the low activation energy for desorption of InI_3. Both BI_3 and BBr_3 provide high etch rates for InGaP under ICP conditions, with the former producing faster rates. These rates are strongly dependent on source power, rf power and plasma composition, and etched surface morphologies improve with increasing BI_3 or BBr_3 content in the discharge. AlInP has very low etch rates in both chemistries due to the involatile Al etch products, and provides an excellent etch stop for InGaP or AlGaP. Chuck dc bias decreases with increasing BI_3 content at fixed source power, but increases with increasing BBr_3 content, which indicates that BI_3 ionizes more readily than Ar and BBr_3. Etch selectivities above 10 are obtained for InGaP over SiO_2 and SiN_x in BI_3 discharges.

ICl provided the fastest etching for InGaP (~2.0μm/min) and AlInP (1.6μm/min) under ECR conditions. Etching achieved with ICl and IBr was not strongly dependent on microwave power in the range 400~1000W, suggesting that the ICl and IBr are easily dissociated and thus provide a high density of reactive neutrals. The rates are significantly faster with ICl under all conditions, consistent with the higher volatilities of the chloride etch products. The etched surface morphologies are a strong function of microwave power and rougher above ~750W, where photoresist mask degradation is also apparent even for short plasma exposures.

In summary, CH_4/H_2-based chemistry appeared to be not suitable for the etching of compound semiconductors in high density plasma tools (ICP, ECR), whereas Cl_2-based chemistries is capable of providing good conditions for the etching of InGaAlP system at a rather high ion energy (>-100V dc) with reasonable results in terms of etch rate, surface morphology and surface chemistry. New plasma chemistries based on iodine and bromine was comparable to the Cl_2-based chemistry in every respect, but care should be taken in handling these gases because of their corrosive nature. As diagnostic tools, Optical Emission Spectroscopy (OES) and mass spectrometry proved to be useful in detecting plasma species as a function of process variables such as (gas composition, source power, ion energy and pressure). However, one concern is that it is hard to detect etch products with mass spectrometry due to the relatively low sensitivity, leading to a difficulty in specifying the surface reaction mechanism. Moreover, OES, applied to ICP tools, is not capable of analyzing plasma on the surface, due to the geometry of chamber.

LIST OF REFERENCES

1 T R Hayes in InP and Related Materials-Processing, Technology and Devices, ed A. Katz (Artech House, Norwood, MA 1992)

2. J M Kuo, Thin Solid Films 231 158 (1993)

3 M J Hafich, H Y Lee, T E Crumbaker, T. J Vogt, P Silvestre and G Y Robinson, J Vac Sci Technol. B 10 969 (1992)

4 K. Ozasa, M Yuri and H Matsunami, J. Cryst Growth 102 31 (1990)

5 Y J Chan, D Pavlidis, M Razheghi and F Omnes, IEEE Trans Electron. Dev ED 37 2141 (1990)

6 J M. Kuo, and Y J Chan, J Vac Sci Technol B 11 976 (1993).

7 M J Mondry and H Kroemer, IEEE Electron Dev Lett. EDL-6 175 (1985)

8 M O Watanabe and Y Ohba, Appl. Phys Lett. 50 906 (1987)

9 W Liu and S K Fan, IEEE Electron Dev Lett. EDL-13 510 (1992)

10 S L Delage, M. A. DiForte-Poisson, H Blanck, C Brylinski, E. Chartier and P Collot, Electron Lett 27 253 (1991)

11 W Pletschen, K H Bachem and T Lautybach, Proc. Mat Res Soc Symp Proc 240 493 (1992)

12. W S Hobson, F Ren, J R. Lothian and S J Pearton, Semicon. Sci. Technol 7 598 (1992)

13 C R Abernathy, F Ren, P Wisk, S J Pearton and R. Esagui, Appl Phys Lett 61 1092 (1992)

14 M Ikeda, Y Mori, H. Sato, K. Kaneko and N Watanabe, Appl Phys Lett. 47 1027 (1985)

15 A. Kikuchi, Y. Kaneko, J Nomura and K Kishino, Electron Lett. 26 1668 (1990)

16. A. Gomyo, T. Suzuki, K. Kobayashi, S. Kawata and I. Hino, Appl. Phys. Lett. 50 673 (1987).

17. K. Kishino, A. Kikuchi, Y. Kaneko and I. Nomura, Appl. Phys. Lett. 58 1822 (1991).

18. W. S. Hobson, Proc. Symp. Wide Bandgap Semiconductors and Devices (ECS, Pennington, NJ) pp. 26-42 (1995).

19. S. J. Groves, J. N. Walpole and C. J. Missaggia, Appl. Phys. Lett. 61 255 (1992).

20. A. W. Hanson, S. A. Stockman and G. E. Stillman, IEEE Electron. Dev. Lett. 14 25 (1993).

21. D. P. Bour, in Quantum Well Lasers, ed. P. S. Zory (Academic Press, NJ 1993) PP. 415-460.

22. See for example, Surface Emitting Semiconductor Lasers and Alloys, ed. G. A. Evans and J. M. Hammer.

23. CRC Handbook of Chemistry and Physics (CRC Press, Boca Raton, FL 1990).

24. U. Niggebrugge, M. Klvg and G. Ganvs, Int. Phys. Conf. Ser. 79 367 (1985).

25. S. J. Pearton, C. R. Abernathy, P. Wisk and F. Ren, J. Appl. Phys. 74 1610 (1993).

26. F. Ren, J. R. Lothian, S. J. Pearton, C. R. Abernathy, P. Wisk, T. Fullowan, B. Tseng, S. N. G. Chu, Y. K. Chen, L. Yang, S. Fu, R. Brozovich, H. H. Lin, C. L. Henning and T. Henary, J. Vac. Sci. Technol. B 12 2916 (1994).

27. F. Ren, J. R. Lothian, W. S. Hobson, J. Lopata, J. Caballero and S. J. Pearton, Appl. Phys. Lett. 67 2497 (1995).

28. J. G. van Hassel, C. M. van Es and P. A. M. Nouwens, Electron. Lett. 31 834 (1995).

29. F. Ren, J. R. Lothian, W. S. Hobson, J. Lopata, J. Caballero and S. J. Pearton, Appl. Phys. Lett. 67 2497 (1995).

30. J. W. Lee, J. Hong and S. J. Pearton, Appl. Phys. Lett. 68 847 (1996).

31. S. Thomas III, K. K. Ko and S. W. Pang, J. Vac. Sci. Technol. A 13 894 (1995).

32. K. K. Ko and S. W. Pang, J. Electrochem. Soc. 11 3945 (1995).

33. D. C. Flanders, L. D. Pressman and G. Pinelli, J. Vac. Sci. Technol. B 8 (6), Nov/Dec (1990).

34 S J Pearton, Int J Mod. Phys B8 1781 (1994)

35 I. Adesida, K. Nummila, E. Andideh, J. Hughes, C Caneau, R. Bhat and R. Holmstrom, J Vac Sci. Technol. B8 1357 (1990)

36 S J Pearton, U K. Chakrabarti, W S Hobson, C. R. Abernathy, A. Katz, F Ren, T. A Fullowan and A. P. Perley, J Electrochem Soc. 139 1763 (1992)

37 C R Abernathy, J Vac. Sci. Technol. A11, 883 (1993)

38 W S Hobson, Mater Res Soc. Symp Proc 300, 75 (1993)

39 T. R. Hayes, U K. Chakrabarti, F A. Baiocchi, A. B. Emerson, H S Luftman, and W C Dautremont-Smith, J. Appl. Phys. 68, 715 (1990)

40 T R. Hayes, M. A. Dreisbach, P M Thomas, W C Dautremont, and L. A Heimbrook, J. Vac Sci Technol B7, 2608 (1989)

41 Fransis Teyssandier and Mark D Allendorf, J Electrochem Soc 6, 2167 (1998)

42 G Y. Adusei and A Fontijn, J Phys Chem 97, 1409 (1993)

43 D L Baulch, J Duxbury, S J Grant and D C Montague, J Phys. Cem Ref Data, 10, Suppl. 1 (1981)

44 R J Shul, G B McClellan, R D. Briggs, D J. Rieger, S J. Pearton, C. R. Abernathy, J W. Lee, C. Constantine and C Barratt, J Vac Sci Technol. A15 673 (1997)

45 F Ren, J R Lothian, J M Kuo, W S Hobson, J Lopata, J. A Caballero, S J Pearton and M W Cole, J Vac Sci Technol. B14 1203 (1995)

46 F Ren, W S Hobson, J R. Lothian, J. Lopata, J A. Caballero, S J Pearton and M W Cole, Appl. Phys Lett 67 2497 (1995)

47 M Vernon, T R. Hayes and V. M Donnelly, J Vac Sci Technol A10 3499 (1992)

48 G A Vawter and C I. H Ashby, J Vac Sci Technol 12 3374 (1994)

49 D G Lisban and E. L. Hu, Appl Phys Lett 56 1667 (1990)

50 S Dzioba, S Jatar, T V Herak, J P D Cook, J Marks, T Jones and F R Shepherd, Appl Phys Lett. 62 2486 (1993)

51 J Hong, J W Lee, C R Abernathy and S J Pearton, J Elect Mat 9, (1996)

52. J W Lee, R. Crockett, and S J Pearton, J. Vac Sci Technol B, 1752 (1996)

53 J Hong, J W Lee, C. J Santana, C R Abernathy, E. S Lambers, S J Pearton, W S Hobson, and F Ren Solid-state Electron., 39, 1406 (1996)

BIOGRAPHICAL SKETCH

Jin Hong was born in Chung Mu, Korea, on May 13, 1967. After graduating from high school, he entered the Hanyang University, located at Seoul Korea in 1986. He got a B. S. in Inorganic Materials Engineering in 1990.

He enrolled in the University of Florida in August 1994 and received a M. S. degree in Materials Science and Engineering in May 1996, under Prof. Stephen J. Pearton, and is completing his Ph. D. degree in Materials Science and Engineering under the same adviser.

He has worked for Sandia National Laboratories as an intern and is author of more than 35 journal papers. He was honored with a Korean Student Research award for his outstanding work.

He will work for Samsung Electronics Semiconductor in Korea.

I certify that I have read this study and that in my opinion it conforms to acceptable standards of scholarly presentation and is fully adequate, in scope and quality, as a dissertation for the degree of Doctor of Philosophy

Stephen J. Pearton, Chairman
Professor of Materials Science and Engineering

I certify that I have read this study and that in my opinion it conforms to acceptable standards of scholarly presentation and is fully adequate, in scope and quality, as a dissertation for the degree of Doctor of Philosophy

Cammy R. Abernathy
Professor of Materials Science and Engineering

I certify that I have read this study and that in my opinion it conforms to acceptable standards of scholarly presentation and is fully adequate, in scope and quality, as a dissertation for the degree of Doctor of Philosophy

Kevin S. Jones
Professor of Materials Science and Engineering

I certify that I have read this study and that in my opinion it conforms to acceptable standards of scholarly presentation and is fully adequate, in scope and quality, as a dissertation for the degree of Doctor of Philosophy

Rajiv K. Singh
Professor of Materials Science and Engineering

I certify that I have read this study and that in my opinion it conforms to acceptable standards of scholarly presentation and is fully adequate, in scope and quality, as a dissertation for the degree of Doctor of Philosophy

Fred Sharifi
Associate Professor of Physics

This thesis was submitted to the Graduate Faculty of the College of Engineering and to the Graduate School and was accepted as partial fulfillmeot of the requirements for the degree of Doctor of Philosophy

December, 1998

Winfred M Phillips
Dean, College of Engineering

M J Ohanian
Dean, Graduate School